94 c30

AN IMPROVED NEUTRAL WIND MODEL WITH PREDICTIVE CAPABILITIES

by

Kathlene R. Dowdy

A thesis submitted in partial fulfillment
of the requirements for the degree

of

MASTER OF SCIENCE

in

Physics
(Upper Atmospheric Option)

Approved:

Kent L. Miller
Dr. Kent L. Miller
Major Professor

B G Fejer
Dr. Bela G. Fejer
Committee Member

W. Farrell Edwards
Dr. W. Farrell Edwards
Committee Member

James P. Shaver
Dr. James P. Shaver
Dean of Graduate Studies

UTAH STATE UNIVERSITY
Logan, Utah

1993

ACKNOWLEDGMENTS

I am indebted to Dr. Kent Miller for allowing me to assist in this research. I appreciate all the patience, advice, discussion, and assistance he provided throughout the course of this project and his unwavering faith in my abilities, without which this paper would not be in existence today. I would like to thank Dr. Bela Fejer and Dr. Farrell Edwards for their continued patience and support. My thanks also go to thank Horng-Yu Wu for the counsel that he provided me, and to Dana Swensen for her encouragement.

I would like to thank Dr. Craig Tepley and Dr. Roger Burnside for the Arecibo Fabry-Perot Interferometer data used in this study, and Dr. Cassandra Fesen for the data from the Thermosphere/Ionosphere General Circulation Model (TIGCM). This study also made use of the CEDAR Data Base at the National Center for Atmospheric Research, which is supported by the National Science Foundation and the National Geophysical Data Center (NGDC; Dr. Raymond Conkright). The Arecibo Observatory is operated by Cornell University under cooperative agreement with the National Science Foundation, and the Millstone Hill Fabry-Perot Interferometer is supported by the National Science Foundation.

I would also like to thank my friends for the moral

support they provided during my course of study. I extend a special thanks to my mom, who supported and encouraged me throughout the years. And finally, I dedicate this work to my dad, who enabled me to obtain my education.

Kathlene R. Dowdy

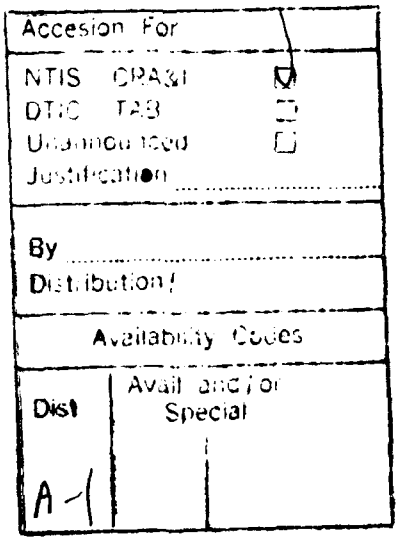

CONTENTS

LIST OF FIGURES

ABSTRACT

An Improved Neutral Wind Model
With Predictive
Capabilities

by

Kathlene R. Dowdy, Master of Science
Utah State University, 1993

Major Professor: Dr. Kent L. Miller
Department: Physics

It has been noted that one of the more essential ingredients of any model of the F2 region of the ionosphere is an accurate estimate of the meridional neutral winds. Inaccurate neutral wind values can drastically change the model's results. Since direct measurements have been difficult to make on a global scale, obtaining wind values has been a difficult problem.

A servo model was developed at Utah State University to calculate the meridional neutral winds from the height of the F2 peak. This model incorporated the Mass Spectrometer Incoherent Scatter model to represent the neutral atmosphere and the International Reference Ionosphere to depict the height of the F2 peak. The servo model was designed to allow the input of F2 peak heights if desired.

The Utah State University Servo model utilized a data base of diurnal coefficients created to compensate for changes in ion loss at different middle latitudes and for varying solar and geomagnetic conditions. The Utah State University Servo model proved a quick, valuable tool in calculating mid-latitude, meridional neutral winds under geomagnetically quiet conditions. (87 pages)

CHAPTER I

INTRODUCTION

Many models exist to compute the density profiles and dynamics of the ionosphere and thermosphere. They range from empirical models based on extensive data bases [Bilitza, 1990] to first-principles models that derive ionospheric parameters from photochemistry [Richards and Torr, 1985; Sojka and Schunk, 1985]. The accuracies of their input parameters and their basic assumptions limit these models. Most of these models require a knowledge of geomagnetic and solar activity levels, as well as a description of the basic state of the atmosphere. One of the more critical input parameters for the first-principles models is the component of the neutral wind that is parallel to the geomagnetic meridian. The current uncertainty in our knowledge of the neutral winds is often the limiting weakness to the accuracy of these models. This thesis describes the development of a model which can provide an accurate estimate of the meridional neutral wind.

One model developed to represent the neutral winds is the servo model. Rishbeth [1967] developed this model to provide a simple model of the behavior of the F2 region of the ionosphere using minimal computer time. Its simplicity lies in the fact that it deals only with the height of the maximum electron density in the F2 layer (F2 peak)

[Rishbeth et al., 1978]. By assuming no vertical winds, the F2 peak occurs at a balance height between production, loss, and diffusion of the ionization. The change in height of the F2 peak produces a change in the chemical and diffusive equilibrium. Downward diffusion increases when the layer rises, retarding any further upward motion of the layer. Conversely, recombination rates increase when the layer lowers, opposing any further downward motion [Rishbeth and Garriott, 1969]. This model assumes that electric field effects are small (which is not an accurate assumption at low latitudes). Comparison studies performed by Miller et al. [1987] and Buonsanto et al. [1989] showed that for quiet geomagnetic periods at mid-latitudes, the electric field effects were slight.

The purpose of this paper is to perform a literature review to summarize the general characteristics of the atmosphere; to provide a background of the development of a servo model at Utah State University (USU) and to describe this model; to perform a limited comparison of its results; and to offer recommendations for future work.

In my research, I developed a USU Servo model patterned after Rishbeth et al. [1978], to calculate the meridional neutral winds from the height of the F2 peak. A meridional neutral wind is the component of the neutral wind that is parallel to the horizontal component of the Earth's magnetic field.

A previous servo model [Ballard, 1991] developed to calculate mid-latitude, meridional neutral winds for geomagnetically quiet conditions from F2 peak layer heights was written in BASIC programming language. Maximum electron density heights were required to be input into this program.

I have incorporated many changes and improvements into this first USU Servo model. This program is written in FORTRAN and has the capability to run quickly on a personal computer. This updated USU Servo model can be run in an interactive mode or by creating a file consisting of the desired input parameters. The Mass Spectrometer Incoherent Scatter (MSIS) model [Hedin, 1987] has been incorporated into the USU Servo model to represent the neutral atmosphere. This model also incorporates the International Reference Ionosphere (IRI) [Bilitza et al., 1987] to depict F2 layer heights. It has the added capability to use measurements of the height of the F2 peak as well.

A significant change in the model is the derivation of diurnal coefficients from the Field Line Interhemispheric Plasma (FLIP) model [Richards and Torr, 1985]. Balance heights were obtained by inserting zero wind values into the FLIP model at numerous locations for various solar and geomagnetic conditions. These balance heights were then used to calculate diurnal coefficients for these locations and conditions. This created a data base for interpolating

diurnal coefficients for mid-latitude locations for different solar and geomagnetic conditions. This process replaces the balance height adjustment made in the previous USU Servo model. It compensates for changes in chemical and diffusive loss of ions at different mid-latitude locations and ionospheric conditions.

The results of the model are compared with Fabry-Perot Interferometer data, incoherent scatter radar data, and independent neutral wind models. The validity of using the IRI to predict wind speeds is also evaluated.

The USU Servo model is a quick, valuable tool in calculating mid-latitude, meridional neutral winds under geomagnetically quiet conditions.

CHAPTER II

REVIEW OF LITERATURE

Vertical Structure of the Atmosphere

The Earth's atmosphere is usually viewed as being divided in terms of its vertical structure. The important parameters in this division are pressure, temperature, density, and chemical composition.

Pressure

The pressure of the atmosphere is simply the weight of the air above a unit area. At sea level, the average pressure is roughly 10 N/cm^2 (1000 millibars). Pressure decreases exponentially with height. At roughly 48 km, the pressure is approximately one-tenth of one percent of sea level pressure [Lutgens and Tarbuck, 1986]. The gases that compose the atmosphere extend for thousands of kilometers beyond the Earth's surface, making the boundaries of the atmosphere difficult to define.

Temperature

The simplest method of dividing the Earth's atmosphere is based on temperature. Generally, temperature decreases with increasing height. The decrease in temperature per kilometer of altitude is called the lapse rate. This method of differentiating the atmosphere distinguishes four main regions: the troposphere, stratosphere, mesosphere,

and thermosphere.

The troposphere is the region closest to the Earth's surface and extends to approximately 15 km. It is characterized by a decrease in temperature with height and a lapse rate of approximately 6.5. Absorption of solar radiation and convection govern the temperature at these altitudes.

The stratosphere lies between 15 and 50 km. From 12-20 km, the temperature remains relatively constant. At this point, the temperature starts to increase sharply with a lapse rate of around -1.7. This is due to the high concentration of ozone (maximum concentration at about 25 km) which absorbs ultraviolet radiation from the sun.

In the mesosphere (50-90 km), temperatures again decrease with altitude and the lapse rate is roughly 2.3. The decreased ozone concentration and the increase in carbon dioxide with its radiative cooling effects account for this change [Rishbeth and Garriott, 1969].

The thermosphere extends from 90 km to around 800 km, although it has no well-defined upper boundary. Due to the absorption of ultraviolet solar radiation and a main heat loss mechanism of downward convection, the neutral temperature begins to increase dramatically to a few thousand degrees. Here the lapse rate is approximately -10.

The uppermost fringes of the atmosphere constitute the

exosphere, starting at approximately 800 km. It can be described as quasi-isothermal. The major components of this area are hydrogen (H) and helium (He).

Electron Density

In addition to the atmospheric regions defined by varying temperature rates, other layers are also recognized. The ionosphere is a region of the Earth's atmosphere that is composed of a partially ionized gas. A significant portion of the ionosphere exists within the thermosphere. The ionosphere extends from approximately 50 km to around 650 km (the lower and upper boundaries remain relatively undefined). Free electrons are suitably abundant in this region to influence radio wave propagation [Rishbeth, 1988]. Above this region is the magnetosphere (1500 km), where the Earth's magnetic field is the controlling force.

The ionosphere is divided into three layers based on varying electron density: D, E, and F layers. The F layer is further divided into the F1 and F2 layers. The layering is due to the ionization of the dominant molecular or atomic species and the depth of penetration of the ionizing radiation (unit optical depth). The ionosphere is where the radiation is attenuated to a fraction of its original intensity [Rishbeth and Garriott, 1969]. There is an altitude of maximum density in each layer, above and below

which the ionization density tends to decrease.

The D layer extends from 50-90 km. The average electron density ranges from 10^2-10^4 cm^{-3}, with a maximum density at noon of about 1.5 x 10^4 cm^{-3}. This layer virtually disappears at night. The peak of the D region ionization is usually around 90 km, but can be lower following solar disturbances. A principal source of ionization in the D layer is the H Lyman α emission line (1216 Å), absorbed by nitric oxide (NO) [Rishbeth and Garriott, 1969].

The E layer ranges from 90-150 km. The average electron density is around 10^5 cm^{-3}, with a noontime maximum of 1.5 x 10^5 cm^{-3} and 10^4 cm^{-3} at night. This peak occurs at about 110 km [Rishbeth and Garriott, 1969]. A main source of E layer ionization is the absorption of extreme ultraviolet (EUV) radiation (911-1027 Å) by molecular oxygen (O_2) [Rishbeth and Garriott, 1969].

The F layer, extending from approximately 150-650 km, is a combination of two slightly different regimes: the F1 region (150-200 km) and the F2 region (200-650 km). The F1 region is basically a transition layer between the E and the F2 layers, although the F1 layer also has an ionization peak. In the F1 layer, a maximum electron density of 2.5 x 10^5 cm^{-3} occurs at noon (becoming absent at night), with an average density of 10^6 cm^{-3}. The peak density occurs at 200 km. For the F2 layer, a maximum electron density at noon

of 10^6 cm^{-3} occurs, decreasing to 10^5 cm^{-3} at night. The height of this maximum density is around 300 km. A principal source of ionization in the F layer is the absorption of EUV radiation (170-911 Å) by atomic oxygen (O) [Rishbeth and Garriott, 1969].

The concentration of ions and electrons varies from day to night, since the main source of ionization is through solar photoionization. During the night, the D and E layer ion densities weaken. The ion concentration in the F layers does not change as rapidly since the density of the atmosphere is lower and ions and electrons do not meet and combine as rapidly as at lower altitudes of higher density. Electron density and peak heights are also highly variable due to seasonal and solar cycle variations. Electron densities in the F2 region also increase/decrease depending upon the season [Rishbeth, 1988].

Chemical Composition

The mid-latitude ionosphere is described as a buffer zone between the dynamic processes of the high-latitudes, where magnetospheric convection and auroral processes exert a strong influence, and the low-latitudes, where large-scale neutral gas-plasma interactions occur [Kelley, 1989]. (Plasma is defined as a gas which contains nearly equal numbers of positive ions and electrons, and is therefore nearly neutral.)

There are two principal processes that determine the characteristics of the ionosphere: production and loss of ionization, and the transport of ionization. The absorption of radiation from the sun causes temperature increases in the thermosphere, production of ions and electrons through ionization, and dissociation of atmospheric gases. The diffusion of ionized particles constitutes an important vertical transport process in the F region. The height of the maximum density of the F region (the F2 peak) occurs at a balance height between these processes. Below the F2 peak, the ionization profile is determined by chemical production and loss processes. Above the F2 peak, diffusion dominates. The height of the F2 peak can be changed by the neutral winds and by electric field effects.

Conservation of mass dictates that the rate of change of the density of a species must equal its production minus its loss and the change due to transport. During sunrise, the change in the density with time is approximately equal to the production rate. At midday, there is a balance between the production and loss rates below the height of the peak electron density. The change in density at night is roughly equal to the loss rate.

Production

Solar photoionization is the principal ion production

process in the ionosphere. Ionization is attained by the absorption of solar EUV and X-ray radiation. Photons react with neutrals, creating ions, as outermost orbital electrons are set free. The rate of photoionization is proportional to the product of the number density of the gas and the intensity of the radiation.

Corpuscular ionization produces ions and electrons through collisions of the neutral particles and energetically charged particles which enter the atmosphere at high latitudes. The energy of these particles determines their depth of penetration into the atmosphere [Rishbeth and Garriott, 1969]. Convection causes this energy to extend towards the equator and to affect the middle latitudes during geomagnetic disturbances.

Negative ions dominate in the D region and are formed primarily through electron-neutral molecular collisions. They include O^-, O_2^-, O_3^-, and NO_2^-. The principal ion constituents are NO^+ and O_2^+ [Kelley, 1989]. In the D region, negative ions outnumber the electrons, especially at lower altitudes and at night. The electron density is less than the positive ion density. Few atomic ions exist. The principal production processes in this region are solar photoionization and corpuscular ionization. Absorption of solar Lyman alpha (1216 Å) radiation by NO and solar X-ray radiation are the main photoionization sources. Cosmic ray radiation also affects the D region. The contribution of

these energetic particles becomes important below 70 km. Cosmic X-rays from X-ray stars provide a source of weak ionization at night as well. Electron attachment to O and O_2 also forms negative ions [Rishbeth and Garriott, 1969].

The major components in the E region are O_2^+ and NO^+ [Kelley, 1989]. Molecular ions dominate in these layers since the electron density is reduced and the lifetime of an atomic ion becomes shorter while the molecular ions last longer [Rishbeth and Garriott, 1969]. The main ionization sources are the Lyman beta (1026 Å) emission line, EUV radiation (911-1027 Å), O_2 ionized by wavelengths greater than 1027 Å, and soft X-ray radiation (10-70 Å). corpuscular radiation is not a significant source, but electrons between 1-30 keV can cause some nighttime and auroral sporadic E ionization (thin patches of ionization overlaid on the regular E layer) [Rishbeth and Garriott, 1969].

The major ion constituents in the F1 region are O^+ and NO^+. The primary components of the F2 region are O^+ and N^+. The main sources (emission lines) of solar photoionization in the F region are from the He II (304 Å) and He I (584 Å) radiations, EUV radiation (170-911 Å), O ionized by wavelengths less than 911 Å, and N_2 ionized by wavelengths less than 796 Å [Rishbeth and Garriott, 1969]. Since oxygen is the major neutral constituent of the F region, neutral oxygen atoms react with photons to produce positive

oxygen ions and free electrons. Although corpuscular ionization is not a significant source in the F region, it can be significant during geomagnetic storms and at night when photoionization is absent. In the nighttime F region, He 584 Å and He^+ 304 Å emissions of the geocorona may be a source of weak ionization [Rishbeth and Garriott, 1969].

Loss

Ions, neutrals, and electrons also react together in photochemical processes. Important losses of ionization in the ionosphere are electron-ion recombination, where absorption of solar radiation causes the molecules to break apart by combining with free electrons; ion-atom interchange; and photodetachment of electrons by solar radiation.

Atomic ions usually do not recombine easily with electrons directly. Instead, molecular ions are formed through ion-atom interchange and then combine with electrons through dissociative recombination [Rishbeth and Garriott, 1969].

Photodetachment by visible and long ultraviolet (UV) radiation is another ionization loss mechanism. Negative ions reacting with photons produce atoms and free electrons.

Ionization in the D region is lost through electron-ion and ion-ion recombination processes (three-body and

dissociative), collisional detachment, associative detachment, and photodetachment [Rishbeth and Garriott, 1969].

Although radiative attachment produces negative ions in the E region, there are few present due to their rapid destruction by photodetachment and electron-ion recombination processes. Important loss processes are electron-ion recombination (dissociative), ion-atom interchange, collisional detachment, and photodetachment [Rishbeth and Garriott, 1969].

The most important electron-ion reaction in the F region is dissociative recombination. Positive nitric oxide (NO^+) molecules combine with electrons to produce neutral nitrogen and oxygen atoms. These resultant atoms generally are in an excited state and then lose this extra energy through collisions with other particles, or subsequent radiation, as ultraviolet, visible, or infrared airglow. Photoelectrons lose their energy through collisions close to the point of their formation in the D and E regions. However, in the F region, photoelectrons can travel large distances before losing their energy [Rishbeth and Garriott, 1969]. This non-local heating occurs mostly at high latitudes.

Most of the NO^+ ions in the F region are produced through ion-atom interchange, coupled with dissociative recombination. Positive oxygen ions collide with neutral

nitrogen molecules to create positive nitric oxide ions and nitrogen ions. Positive nitrogen ions combining with neutral oxygen atoms produce the same results.

Photodetachment is largely responsible for the absence of negative ions in the F region. Although negative ions are produced slowly by radiative attachment, they are destroyed rapidly by photodetachment in the daylight and also by ionic recombination [Rishbeth and Garriott, 1969]. Above the F2 peak, ions are lost principally through transport to lower altitudes. Below the F2 peak, ion-molecular reactions are mainly responsible for the loss of ionization [Rishbeth and Garriott, 1969].

Transport

Collision frequency, gravity, and pressure gradients are the main processes responsible for vertical transport of ions and electrons. The collision frequency of ions with neutral particles is large enough below around 130 km to slow the ions appreciably. Therefore, the assumption of constant density within a given volume is valid. However, vertical pressure gradients may move a given volume up or down as a whole. Between 130-300 km, plasma diffusion becomes an important process and remains important throughout the ionosphere. The balance height marks the boundary between altitudes dominated by diffusion (above) and recombination (below). Above 300-400 km, the plasma

becomes essentially collisionless.

At mid-latitudes, vertical transport of the particles up or down occurs along the magnetic field lines. Under ambipolar diffusion, the particles move upward or downward in accordance with their mass, due to gravity. Electrons, being lighter, diffuse faster down a pressure gradient than ions [Kelley, 1989]. This results in the electrons settling above the ions and hence a charge separation. A polarization electrostatic field is produced that stabilizes the charge separation. Then the electrons and ions move together [Schunk, 1983].

Below the F2 peak, production and loss of ionization are the controlling processes. Above the peak, diffusive equilibrium of the dominant species dominates. The diffusion of the electrons is much faster than the ions across a pressure gradient because of their lighter mass [Kelley, 1989]. This process causes a charge separation and tends to destroy any electron pressure gradients. But the diffusion of the electrons is controlled and the ion diffusion is enhanced by the electric field set up by the charge separation [Kelley, 1989]. The electric field is balanced by the pressure gradient. Light minor ions He^+ and H^+ can be accelerated outward by this electric field. This results in a hydrogen gas surrounding the Earth (geocorona) [Kelley, 1989].

The density near the peak of the F2 layer often

increases shortly after sunset, due to transport processes. It then decreases to nighttime values [Richards and Torr, 1985].

The Geomagnetic Field

The Earth's magnetic field surrounds the thermosphere and extends for several Earth radii [Rishbeth and Garriott, 1969]. It originates through currents, driven by thermal convection, in the molten, electrically conducting core of the Earth. The geomagnetic field can be portrayed by a dipole inclined by about 12 degrees to the Earth's axis [Rishbeth, 1988]. The dipole position varies with time and flips over occasionally (roughly every 100,000 years).

The magnetic field lines are inclined at an angle with the Earth's surface (known as the dip angle I). They cross the Earth's magnetic equator at a distance of L Earth radii (L-shell). Each point on the Earth's surface has a conjugate point at the same magnetic latitude on the opposite hemisphere. These geomagnetic field lines are closed in the low and mid-latitudes, but are linked to the Earth's magnetosphere and the interplanetary magnetic field at higher latitudes.

The ionosphere at upper latitudes is greatly influenced by charged particles and electric currents which originate in the magnetosphere. These effects produce the aurora and magnetic storms. The charged particles and

currents enter the ionosphere in the areas surrounding the magnetic poles. Magnetic storms tend to follow solar disturbances. The degree of geomagnetic variability is described by geomagnetic indices (including the Ap index) from measurements made at geomagnetic observation sites [Rishbeth, 1988].

Geomagnetic storms are caused by solar disturbances, especially from areas of solar flares. The energy released from these events travels away from the sun with the solar wind. The impact of this energy on the Earth's magnetosphere causes a compression of the geomagnetic field. Some of this energy also finds its way into the ionosphere, inducing a myriad of effects. Geomagnetic disturbances cause magnetospheric convection increases at high-latitudes to extend equatorward. Collisions between energetic particles precipitated into the atmosphere and the neutrals produce ions and electrons [Rishbeth and Garriott, 1969]. This gives rise to increased heat and momentum sources in mid-latitude regions [Roble, 1983], generating strong neutral winds.

Magnetic storms can result in the reduction of the electron density in the F region (negative storm effects). This happens as a result of collisions between the ions and precipitated charged particles, and the ion-atom interchange and dissociative recombination. Another reason for electron density decreases is the change in the neutral

gas composition. Increases of molecular nitrogen and oxygen densities and concurrent decreases of atomic oxygen density are seen as the main components of these neutral gas changes. Also, negative storm effects can result from displacement and expansion of the ionospheric electron concentration trough region toward lower latitudes [Prlöss et al., 1991].

E Region Dynamo

Tidal forces in the Earth's atmosphere are created by heating through solar EUV and X-ray absorption and by the gravitational effects of the sun and the moon. The absorption of solar EUV and X-rays in the E region and the UV absorption in the ozone layer generate atmospheric tides. These thermal tides propagate upward to produce waves in the atmosphere, which are observed as mainly horizontal wind motions. At night, E region conductivities decrease significantly enough that polarization electric fields develop that transport ions across the magnetic field lines with the neutrals [Rishbeth, 1971]. In the E region, when winds blow across magnetic field lines, the ions can move with the wind, but the electrons are constrained to move along the field lines by the magnetic field. This produces a current (flowing in the opposite direction to the movement of the electrons) that is opposite to the direction of the wind. This current has an

electric field associated with it. An equilibrium state is reached when the electric field's dissipation of charge equals the build-up of charge by the current [Richmond, 1983]. When the wind reverses direction, so does the current and hence the magnetic field. This accounts for daily magnetic variations.

This dynamo region is confined to a narrow range around 100-130 km, where atmospheric conductivity is greatest. The effects of this region are more pronounced during solar minimum. The magnetic fields are mapped to the F region along the geomagnetic field lines where they cause electromagnetic drifts [Rishbeth and Garriott, 1969]. They are also transmitted to the opposite hemisphere, producing symmetry about the Earth's magnetic equator [Richmond, 1983].

Mid-latitude Ionospheric Circulation

Heating due to solar EUV and UV absorption primarily determines the general circulation at mid-latitude F region heights during quiet geomagnetic conditions. However, high-latitude heat and momentum sources influence the circulation during geomagnetic disturbances [Roble, 1983]. The energy provided from these sources produces horizontal temperature variations between the day and night, which create a daytime expansion of the ionosphere, known as the diurnal bulge. This expansion creates a high pressure

region on the sunward side of the Earth. This, in turn, produces horizontal pressure gradients that generate thermospheric winds. When geomagnetically quiet conditions occur, neutral meridional winds are generally poleward during the day, becoming equatorward during the night.

There are numerous external forces that determine the neutral wind velocity, including the Coriolis force, ion drag, molecular viscosity, the pressure gradient force, and gravitational acceleration.

One important parameter is the Coriolis force, due to the Earth's angular rotation. Because of the Earth's rotation about a vertical axis, this apparent force (as viewed from the rotating system) deflects all free-moving particles to the right of their path of motion in the northern hemisphere and to the left in the southern hemisphere. It acts perpendicular to the velocity vector and only changes the direction of motion. The Coriolis force is dependent on latitude, being strongest at the poles and weakening towards the equator, where it becomes nonexistent. The Coriolis force is expressed by the equation:

$$F_c = 2\ \Omega\ X\ U \qquad (1)$$

where Ω is the Earth's angular velocity, and U is the neutral velocity.

Another central force affecting motion is ion drag.

When electric fields cause the ions to move, the ions are restricted to move along the Earth's magnetic field lines, while the neutrals can move across these lines. Ion drag is a frictional force on the neutrals, which is caused by collisions between the neutral particles and the ions. This tends to slow down the neutral particles. Ion drag is controlled by the ion-neutral collision frequency and the neutral wind and ion velocity difference [Rishbeth, 1988]. This force is expressed by the form:

$$F_p = \nu_{ni} \left(\boldsymbol{U} - \boldsymbol{V}_i \right) \qquad (2)$$

where ν_{ni} is the collision frequency between neutral particles and ions, $\mathbf{U}$ is the velocity of the neutrals, and $\mathbf{V}_i$ is the ion velocity.

The molecular viscosity of the air also affects the neutral wind velocity. The viscous drag force is a mechanism that converts the kinetic energy of moving objects into thermal energy (analogous to friction in solids). A force must be exerted to cause one layer of a fluid to slide past another layer. This force is the result of a momentum transfer from particles to a fluid that reduces the velocity gradient. It depends on collisions and is a dissociate process. The energy in a fluid momentum transfer is converted into heat [Kelley, 1989]. This force is represented by the form:

$$F_v = \frac{\mu}{\rho} \nabla^2 \mathbf{U} \qquad (3)$$

where μ is the viscosity coefficient, ρ is the mass density, and $\mathbf{U}$ is the neutral velocity.

The pressure gradient force and gravitational acceleration also play a part. If the atmosphere is subjected to a higher pressure in one region than in another, an imbalance, or pressure gradient, exists (caused by solar differential heating). This inequality produces a net force from the region of higher pressure to the lower pressure region. The vertical pressure gradient is predominantly balanced by the force of gravity. Gravitational acceleration is caused by the force per unit mass exerted on the atmosphere by the gravitational attraction of the Earth.

Neutral Winds

The neutral wind is a balance between the pressure gradient forces, the frictional forces of ion drag and viscosity, the Coriolis force, and gravitational force. The forces per unit mass (accelerations) controlling the neutral wind velocity are combined in the momentum equation:

$$\frac{d\mathbf{U}}{dt} = \mathbf{g} - \frac{1}{\rho} \nabla p - 2\, \boldsymbol{\Omega} \times \mathbf{U} - \nu_{ni} (\mathbf{U} - \mathbf{V}_i) - \frac{\mu}{\rho} \nabla^2 \mathbf{U} \qquad (4)$$

(1) (2) (3) (4) (5) (6)

where the terms are (1) change in neutral velocity with time, (2) gravitational force, (3) pressure gradient force, (4) Coriolis force, (5) ion drag, and (6) viscosity. Since the vertical pressure gradient force is balanced by the gravitational force, the neutral winds are assumed to be horizontal.

The ratio of the Coriolis force to ion drag determines the direction of the neutral wind. In the F region, ion drag is large and the wind is almost parallel to the pressure gradient force. At lower altitudes, the Coriolis force is dominant while ion drag is small, and the neutral wind is perpendicular to the pressure gradient force [Rishbeth, 1988].

The acceleration of the neutral air due to collisions with ions moving under the influence of an electric field can be expressed by the form:

$$\frac{\delta \boldsymbol{U}}{\delta t} = \nu_{ni} \left(\boldsymbol{V}_i - \boldsymbol{U} \right) + \frac{\mu}{\rho} \frac{\delta^2 \boldsymbol{U}}{\delta h^2} \qquad (5)$$

This equation states that the change in the neutral velocity with time is equal to the force applied through ion drag and the viscosity force. Below around 150 km, the neutral-ion collisional frequencies are small. Therefore, there is only a small effect of the acceleration of the neutrals due to ion drag. At these altitudes, tidal motions and gravity waves are more important sources of neutral motion [Rishbeth and Garriott, 1969].

From 200-300 km, the daytime neutral-ion collision frequencies are larger than nighttime values. This allows ion drag to have a larger impact on the neutral wind acceleration without much effect from viscosity. At night, the acceleration is slow and is affected by viscosity [Rishbeth and Garriott, 1969].

Electric fields cause ions to move across the magnetic field lines, which leads to ion drag. The ions set the neutrals into horizontal motion. The ratio of the Coriolis force to ion drag then determines the neutral wind direction. Electric fields are the dominant forces controlling the neutral winds at high latitudes. Also, localized pressure gradients and consequently thermal winds are produced by auroral heating. At these latitudes, pressure gradient forces and ion drag must be considered to be important. However, at lower latitudes thermal winds controlled by solar heating dominate. Near the magnetic equator, electric field effects are again important [Rishbeth, 1988].

At higher altitudes, small-scale velocity gradients are smoothed out by viscosity. As the height increases, the density becomes smaller, making μ/ρ larger, so that $\nabla^2 U$ must become small. This means that the spatial variations of U are suppressed by viscosity, and the neutral wind varies little with height. However, at lower altitudes the density increases and this effect is not seen

[Rishbeth, 1988].

F2 Peak

The maximum electron density in the F region occurs at the F2 peak where chemical processes and diffusive properties balance.

Without neutral winds or electric fields, the F2 peak remains fixed at a balance height. If winds are present, the peak undergoes a vertical displacement and the equilibrium level between chemical and diffusive processes is shifted as well.

The component of the neutral wind parallel to the magnetic field affects the altitude of the peak density of ionization at F region heights through ion-neutral collisions [Rishbeth, 1972]. The neutral wind component parallel to the magnetic field lines accelerates the plasma. The vertical component of the neutral wind then adds to the vertical component of the plasma drift velocity.

During the day, a poleward neutral wind induces a downward ionization drift parallel to the magnetic field. This has the effect of lowering the F2 layer. The ionosphere is driven downward where chemical loss rates are greater and hence the ion density is decreased. A horizontal wind blowing towards the magnetic equator drives the ionization up the magnetic field lines. This pushes

the F layer upward and increases the ion density, thus raising the peak. In the absence of electric fields, the Earth's magnetic field directs the ion motion along the field lines. In this way the neutral wind affects the variability in the height of the F2 peak and the density profile of the F region.

Thermal tidal forces on neutral winds in the F region result from absorption of solar radiation and differential heating of the atmosphere. The temperature of the atmosphere is greater on the sunward side of the Earth than on the dark side. This causes the atmospheric pressure to increase on the sunward side, and the air flows from the area of higher pressure to that of lower pressure. From the reference frame of the rotating Earth, this flow varies periodically, inferring the tides.

Electric fields in the E region also influence the height of the F2 peak through electromagnetic drifts. At low latitudes, the diurnal tide dominates, while the semidiurnal tide dominates at high latitudes [Rishbeth and Garriott, 1969]. These tidal forces generate winds in the E region. It is the motion of these winds across the Earth's geomagnetic field which create electric fields and currents. These electric fields are mapped to the F region along the magnetic field lines. These fields influence the height of the F2 peak through electromagnetic drifts. Eastward electric fields produce upward electromagnetic

drifts (the vertical component of the drift velocity), while westward fields induce downward drifts. Ion drag significantly reduces the influence of these electric field effects on the mid-latitude F2 peak [Rishbeth, 1988].

In high latitudes, horizontal wind movements due to electric fields may dominate. However, at mid-latitudes solar heating dominates the movement of the winds [Rishbeth, 1988].

CHAPTER III

USU SERVO MODEL

Models Incorporated into the USU Servo Model

The USU Servo model utilizes three well respected models to obtain the meridional neutral winds. These are the International Reference Ionosphere (IRI) [Bilitza, 1990], the Mass Spectrometer Incoherent Scatter (MSIS) model [Hedin, 1987], and the Field Line Interhemispheric Plasma (FLIP) model [Richards and Torr, 1985].

The International Reference Ionosphere (IRI) is an empirical ionospheric model and is sponsored by a joint working group of the Committee on Space Research (COSPAR) and the International Union of Radio Science (URSI). This model generates monthly averages of the electron density, electron temperature, ion temperature, and ion composition for geomagnetically quiet conditions in the nonauroral ionosphere from 50 km to 1000 km. Required inputs are geodetic or geomagnetic latitude and longitude, altitude, sunspot number, month, and local or universal time. Major data sources for this model include the worldwide network of ionosondes and incoherent scatter radars [Bilitza, 1990]. The USU Servo model uses the IRI to obtain the height of the F2 peak.

The Mass Spectrometer Incoherent Scatter (MSIS) model

describes the neutral temperature and densities in the upper atmosphere (above 100 km). Developed by Hedin [1987], it is based on extensive data compilation and analysis. Data sources include rockets, satellites, and incoherent scatter radars. Number densities of O, N_2, O_2 and the neutral temperature, derived from the MSIS model, are used in the USU Servo model.

The Field Line Interhemispheric Plasma (FLIP) model is a comprehensive one-dimensional, photochemical model of the ionosphere-plasmasphere system [Richards and Torr, 1985]. Inputs to the FLIP model are neutral temperatures and concentrations from the MSIS model [Hedin, 1987], 10.7 cm solar radio flux, magnetic activity index A_p, location, local time, the solar EUV flux spectrum, the photoionization cross sections, and the total electron impact cross sections. The neutral wind is required as an input to the FLIP model's computation, but can be derived as an option from user-specified values of the height of the F2 layer [Richards and Torr, 1988]. The FLIP model produces plasma densities and temperatures along an entire geomagnetic flux tube, extending from 80 km in the northern hemisphere to 80 km in the southern hemisphere. The USU model utilizes balance heights obtained by entering zero winds into the FLIP model. The balance heights are used to calculate diurnal coefficients (c). This coefficient was introduced by Rishbeth [1967] as an empirical constant of

order unity. Its purpose is to account for the effects of transport processes and loss mechanisms at the F2 peak. These diurnal coefficients were calculated for magnetic latitudes from 30-60 degrees in both the northern and southern hemispheres and for both high and low F10.7 flux and Ap values at the equinoxes and solstices.

Servo Model Equations

Rishbeth introduced the servo model in 1967 [Rishbeth, 1967] to study the effect of plasma drift velocity on the F2 peak. The equations were rederived in a paper published in 1978 [Rishbeth et al., 1978]. The USU Servo model is based on the underlying principles and equations developed by Rishbeth et al. [1978].

The USU Servo model is based on the following principles set forth by Rishbeth [1967] and Rishbeth et al. [1978]:

(1) By assuming no applied vertical drift, the F2 peak is situated at a balance height between chemical processes and diffusion.

(2) Under the influence of a vertical drift due to neutral winds and electric fields, this equilibrium position of the F2 peak is shifted in altitude and varies with the applied drift.

(3) The F2 peak displaces to a new equilibrium height at a rate defined by diffusion and loss.

The fundamental equations of the servo model are derived by Rishbeth et al. [1978]. Since the USU Servo model is based on these equations, they are reproduced here.

The continuity equation states that the change in density of a species equals its production rate minus its loss rate and the change due to transport. This equation is expressed in the form:

$$\frac{\partial N}{\partial t} = q - \beta N - \frac{1}{H} \frac{\partial}{\partial z} (NV_z) \qquad (6)$$

where N is the electron number density, q is the electron production rate, β is the loss coefficient, H is the scale height (or "thickness of the atmosphere" [Rishbeth, 1988]), z is the reduced height (z = 0 at the balance height), and V_z is the vertical plasma velocity (positive upwards). Horizontal transport terms are neglected due to the assumption of horizontal stratification.

In the F2 region, the ions are principally atomic and the ion-atom interchange reaction controls the rate of loss, which is linear. Therefore, we can assume a beta recombination loss regime ($L = \beta N$).

First multiply equation (6) by H and integrate from $z = z_m$ (F2 peak) to $z = \infty$ (top of the ionosphere):

$$H \frac{\partial}{\partial t} \int_{z_m}^{\infty} N \, dz = H \int_{z_m}^{\infty} (q - \beta N) \, dz - \Phi_\infty + N + N_m \left(V_{zm} - H \frac{dz_m}{dt}\right) \tag{7}$$

where Φ_∞ is the vertically upward plasma flux at the top of the ionosphere (the limiting value of NV_z). The term (V_{zm} - H dz_m /dt) is the relative vertical plasma velocity at the F2 peak.

Based on the following assumptions:

(1) The topside layer sustains a constant shape that is expressed by the Chapman alpha layer, a = 2.82.

(2) q is proportional to e^{-z}, since the F2 peak is sufficiently above the peak of the production layer.

(3) Since O^+ is principally lost through dissociative recombination ($O^+ + N_2 \rightarrow NO^+ + O$), β is proportional to e^{-kz}, where k is the ratio between the atomic and molecular scale heights, the resulting equation becomes:

$$a H \frac{dN_m}{dt} = q_m H - \frac{\beta_m N_m H}{k} - \Phi_\infty + N_m \left(V_{zm} - H \frac{dz_m}{dt}\right) \tag{8}$$

where aHN_m is the height-integrated ion content of the topside layer.

By assuming the F2 layer is isothermal, the peak vertical plasma drift velocity is written:

$$V_{zm} = W - \frac{g \sin^2 I}{\nu_m} \tag{9}$$

where W is the applied vertical drift, g is the gravitational acceleration, I is the dip angle, and ν_m is

gravitational acceleration, I is the dip angle, and ν_m is the ion-neutral collision frequency.

Substituting V_{zm} from equation (9) into equation (8), dividing by $N_m H$, and rearranging terms yield:

$$\frac{dz_m}{dt} = \frac{q_m}{N_m} - \frac{\Phi_\infty}{N_m H} - \frac{a}{N_m}\frac{dN_m}{dt} - \frac{\beta_m}{k} - \frac{g \sin^2 I}{\nu_m H} + \frac{W}{H} \quad (10)$$

Rishbeth et al. [1978] uses a good approximation of the continuity equation to solve equation (10), giving:

$$\frac{dN_m}{dt} = q_m - c\,\beta_m N_m - \frac{\Phi_\infty}{a H} \quad (11)$$

This assumes that the flux (Φ_∞) is distributed evenly over the thickness of the topside layer (aH). It also introduces the constant c to combine transport and loss terms.

Substituting dN_m/dt from equation (11) into equation (10) yields:

$$\frac{dz_m}{dt} = (1 - a)\frac{q_m}{N_m} + \frac{(kac - 1)\,\beta_m}{k} - \frac{g \sin^2 I}{\nu_m H} + \frac{W}{H} \quad (12)$$

The equilibrium level is found by assuming W=0, dz_m/dt=0, and no flux. Solving equation (11) for N_m gives:

$$N_m = \frac{q_m}{c\,\beta_m} \quad (13)$$

Substituting N_m into equation (12), with the above assumptions, and solving for β_e, produces a ratio of

equilibrium loss coefficient and an equilibrium ion-neutral collision frequency:

$$\beta_e = \frac{g \sin^2 I}{\nu_{in} H(\frac{kc-1}{k})} \tag{14}$$

Using the relationships that $q_m=q_e\exp(-z_m)$, $\beta_m=\beta_e\exp(-kz_m)$, and $\nu_m=\nu_e \exp(-z_m)$, and substituting these relationships along with β_e from equation (14) into equation (12), gives:

$$\frac{dz_m}{dt} = (1 - a) \frac{q_e \exp(-z_m)}{N_m} + (\frac{g \sin^2 I}{\nu_e H}) \frac{[kac -1}{[kc - 1} \exp(-kz_m) - \exp(z_m) \,]] + \frac{W}{H} \tag{15}$$

Using equation (13) to approximate N_m, equation (15) becomes:

$$\frac{dz_m}{dt} = (\frac{g\sin^2 I}{\nu_e H}) \, [\exp(-k\, z_m) - \exp(z_m)] + \frac{W}{H} \tag{16}$$

Solving for a steady drift W ($dz_m/dt=0$) yields:

$$W = (\frac{g\sin^2 I}{\nu_e}) \, [\exp(z_m) - \exp(-kz_m)] \tag{17}$$

Equation 17 is nonlinear due to its exponential functions of height. To obtain a simplified solution for negligible changes in height, a linear form of this equation (17) can be used:

$$W_1 \approx \left(\frac{g \sin^2 I}{\nu_e}\right) (z_m) (1 + k) \qquad (18)$$

where $z_m=(h_m-h_0)/H$.

By combining these equations (16 and 17) for the applied vertical drift and assuming W is due only to the neutral wind (neglecting electric field effects), the neutral wind is found from the following equation:

$$U_p = \frac{-W}{\cos I \sin I} \qquad (19)$$

where U_p is the poleward meridional neutral wind.

If electric field effects are included, the vertical drift velocity is expressed by the equation:

$$W = V_{\perp p} \cos I - U_p \cos I \sin I \qquad (20)$$

where $V_{\perp p}$ is the poleward perpendicular component of the ion drift velocity (perpendicular to the Earth's magnetic field).

$V_{\perp p} \cos(I)$ can generally be neglected for quiet to moderate geomagnetic conditions [Richards, 1991]. This assumption again leads to equation (19).

Using the trigonometric relation:
$\sin(2\alpha)=2\sin(\alpha)\cos(\alpha)$, and substituting this into equation (19), gives:

$$U_p = \frac{-2W}{\sin 2I} \qquad (21)$$

which is the equation used in the USU Servo model to obtain

the meridional neutral winds.

Electron and plasma temperatures are significantly different in the F region. The plasma temperature is of the form:

$$T_p = \frac{1}{2} \left(T_i + T_e \right) \qquad (22)$$

where T_p is the plasma temperature, T_i is the temperature of the ions, and T_e is the electron temperature [Rishbeth and Garriott, 1969].

The plasma scale height is expressed by the form:

$$H_p = \frac{2\ k\ T_p}{m_i\ g} \qquad (23)$$

where H_p is the plasma scale height, k is Boltzmann's constant, T_p is the plasma temperature, m_i is the ion mass, and g is the gravitational acceleration. This equation assumes that the mean particle mass of the plasma is 1/2 m_i. This is done because the electron mass is negligible [Rishbeth and Garriott, 1969].

Servo Model Procedure

Figure 1 depicts a flow chart of the main USU Servo model processes. Following is a step-by-step discussion of each procedure contained in the servo model:

1. The servo model can be run using either an interactive mode for parameter input or a passive mode. In the

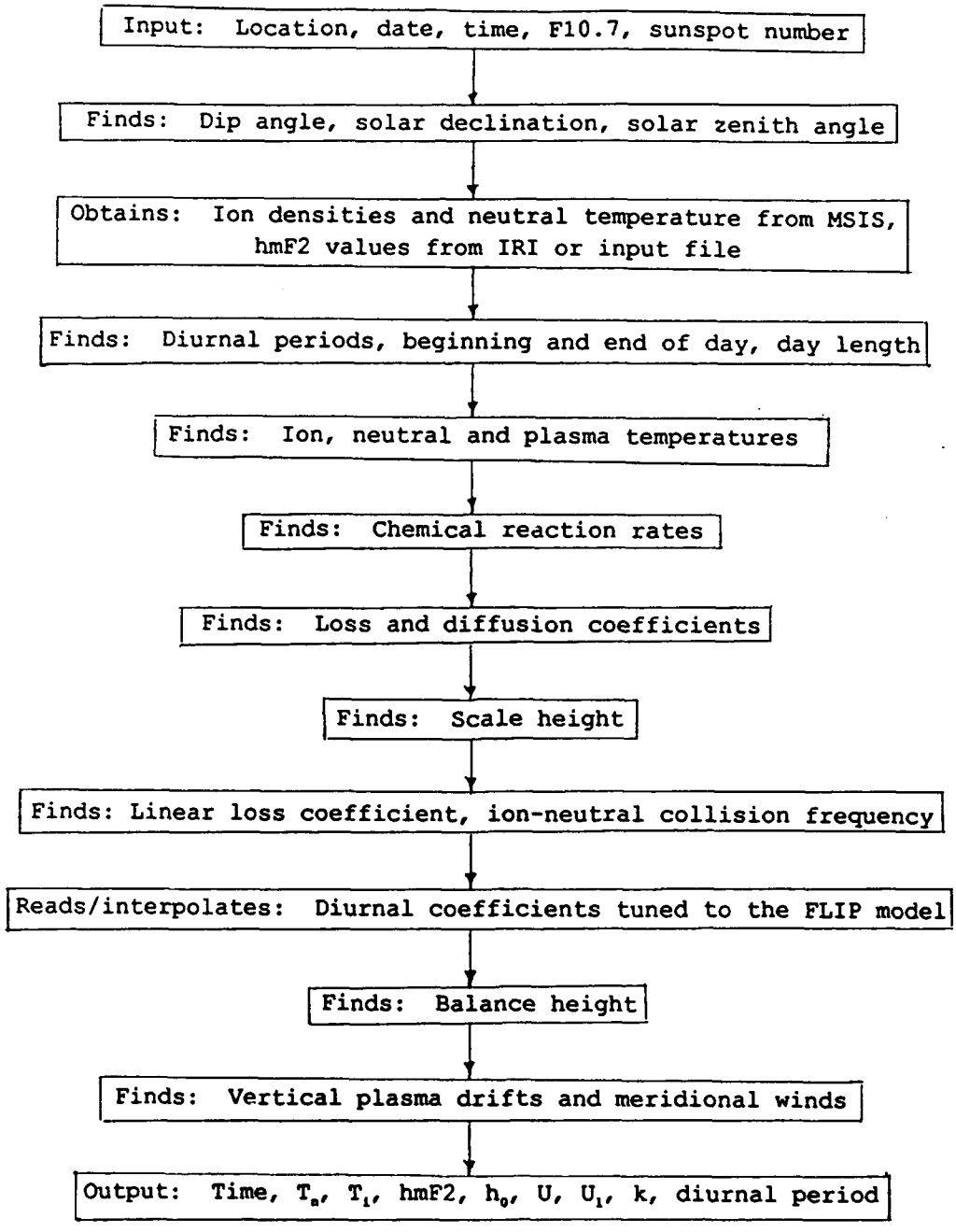

Fig. 1. Flowchart of the main USU Servo model processes.

passive mode a file must be created with the desired input parameters to be read by the servo program. Input parameters into the servo model are the location name, geodetic latitude, geodetic longitude, month, day, year, local time (LT) or universal time (UT), F10.7 solar flux values, and sunspot number.

2. The dip angle (I) may be input if known. Otherwise, it is calculated using a centered dipole approximation:

$$I = \arctan\,[2 \tan\,(\textit{Dip latitude})] \tag{24}$$

where:

$$\textit{Dip latitude} = \frac{M}{\sqrt{(1 - M^2)}} \tag{25}$$

and

$$M = \sin\,(\textit{glat})\,\sin\,(78.5) + \cos\,(\textit{glat})\,\cos\,(78.5)\,\cos\,(\textit{glon} - 291) \tag{26}$$

3. The day of the year (DOY) is calculated.

4. The solar declination is calculated. Solar declination is the angle between the Earth-sun line and the Earth equatorial plane. It can be represented in terms of the day of the year:

$$\textit{SDEC} = .006918 - .399912\cos\,(da) + .070257\sin\,(da) - .006758\cos\,(2\,da) + .000907\sin\,(2\,da) - .002697\cos\,(3\,da) + .00148\sin\,(3\,da) \tag{27}$$

where:

$$da = \frac{2\,\pi\,dd}{365} \tag{28}$$

and

$$dd = 365 - INT\left[\frac{365}{DOY + (365 - 275)}\right]\,[DOY + (365 - 275)] \tag{29}$$

5. Solar zenith angle is calculated. The solar zenith angle at a point p is the angle between the Earth radius through p and the line from p to the sun:

$$SZA\ (t) = \sin\ (glat)\ \sin\ (SDEC) + \cos\ (glat)\ \cos\ (SDEC)\ \cos\ (t) \tag{30}$$

$$SZA\ (t) = \frac{\pi}{2} - \arctan\frac{SZA\ (t)}{\sqrt{1 - SAZ\ (t)^2}} \tag{31}$$

6. An hourly change in the daytime coefficient, which will be called the dayslope, is assigned according to the solar flux value. A daytime steady rate of change is assumed. A zero dayslope assumes a constant daytime coefficient:

   F107 > 150: Dayslope = .05

   80 < F107 < 150: Dayslope = .1

   F107 < 80: Dayslope = .15

7. The dayslope may be changed, if desired.
8. The MSIS subprogram is called, which automatically sets the reference height at 300 km, to obtain number densities (cm^{-3}) for O, N_2, O_2, and the temperature at 300 km.
9. The IRI subprogram may be called to obtain the height

of the F2 peak for each hour, or an alternate file of hmF2 values may be read into the program.

10. Diurnal periods are determined using the solar zenith angle:

Morning:	82 < SZA < 102, SZA decreasing:	X = 3
Daytime:	SZA < 82:	X = 1
Evening:	82 < SZA < 102, SZA increasing:	X = 4
Nighttime:	102 < SZA:	X = 2

11. The hours the day begins and ends, based on solar zenith angles, are determined. The length of the day, based on the zenith angle of the sun, is calculated.

12. Ion temperatures are assigned as a ratio of the neutral temperatures for each hour, based on the solar flux and diurnal periods:

For F107 > 150:

Morning: $T_i = T_n$

Daytime: $T_i = 1.08(T_n)$

Evening: $T_i = T_n$

Nighttime: $T_i = T_n$

For 80 < F107 < 150:

Morning: $T_i = 1.05(T_n)$

Daytime: $T_i = 1.10(T_n)$

Evening: $T_i = 1.05(T_n)$

Nighttime: $T_i = T_n$

For 150 < F107:

Morning: $T_i = 1.15(T_n)$

Daytime: $T_i = 1.02(T_n)$

Evening: $T_i = 1.05(T_n)$

Nighttime: $T_i = 1.10(T_n)$

13. The plasma temperature at the reference height is calculated as the average between the ion and neutral temperatures.

14. Chemical reaction rates are calculated for N_2 and O_2 with O^+ at the reference height for each hour (cm^3/s):

k1: $O^+ + O_2 \rightarrow O^{2+} + O$

$$k_1 = 2.82 \times 10^{-11} - 7.74 \times 10^{-12} \frac{[TR]}{[300]} + 1.073 \times 10^{-12} \frac{[TR]^2}{[300]} - 5.17 \times 10^{-14} \frac{[TR]^3}{[300]} - 9.649999 \times 10^{-16} \frac{[TR]^4}{[300]} \quad (32)$$

k2: $O^+ + N_2 \rightarrow NO^+ + O$

For $T_r \leq 1700$:

$$k_2 = 1.533 \times 10^{-12} - 5.92 \times 10^{-13} \frac{[TR]}{[300]} + 8.6 \times 10^{-14} \frac{[TR]^2}{[300]} \quad (33)$$

For $T_r > 1700$:

$$k_2 = 2.73 \times 10^{-12} - 1.155 \times 10^{-12} \frac{[TR]}{[300]} + 1.483 \times 10^{-13} \frac{[TR]^2}{[300]} \quad (34)$$

15. The loss scale height factor between N_2 and O_2 loss is calculated for each hour:

$$k = \frac{\frac{k_1}{k_2}}{\frac{k_1}{k_2} + \frac{[N_2]}{[O_2]}} (0.25) + 1.75 \quad (35)$$

16. Gravitational acceleration at the reference height is

calculated (m/s^2):

$$g = \frac{9.80 - 2.59 \cos (2\ glat) - .308\ (h_r)}{100} \qquad (36)$$

17. The O^+ scale height H at the reference height is calculated for each hour:

$$H = \frac{8314.3\ T_r}{16\ g\ (1000)} \qquad (37)$$

18. The linear loss coefficient at the reference height is calculated for each hour:

$$\beta = k_1\ [O_2] + k_2\ [N_2] \qquad (38)$$

19. The ion-neutral collision frequency at the reference height is calculated for each hour (s^{-1}):

ν: $(O^+ \rightarrow N_2) + (O^+ \rightarrow O_2) + (O^+ \rightarrow O)$

$$\nu_{in} = 6.82\ X\ 10^{-10}\ [N_2] + 6.64\ X\ 10^{-10}\ [O_2] + 1.7\ [3.67\ X\ 10^{-11}\ [O]\ (\sqrt{T_r})]\ [1 - 0.0278\ \ln\ (T_r)]^2 \qquad (39)$$

20. A subroutine to obtain diurnal coefficients c is called, and the model interpolates these coefficients according to Ap values, geodetic latitude, day of the year, and F10.7 solar flux values. The c values are interpolated between arrays of c values obtained from calculations based on FLIP model balance heights.

21. The nonlinear and linear vertical plasma drift are calculated for each hour:

Nonlinear:

$$W = \left[\exp\frac{h_m - h_0}{H} - \exp\frac{-k\ (h_m - h_0)}{H}\right] \quad \frac{[g \sin^2 I]}{[\nu_{in}]} \qquad (40)$$

Linear:

$$W_I = \frac{(h_m - h_0)\ (1000)\ (k + 1)\ (g)\ (\sin^2 I)}{(\nu_{in})\ (h)\ (1000)} \qquad (41)$$

where h_m is the height of the F2 peak.

22. The nonlinear and linear meridional neutral winds from the vertical plasma drifts are calculated for each hour:

Nonlinear:

$$U = \frac{-2W}{\sin(2I)} \qquad (42)$$

Linear:

$$U_I = \frac{-2W_I}{\sin(2I)} \qquad (43)$$

23. An output file is generated consisting of the time, neutral temperature (T_n), ion temperature (T_i), height of the F2 peak (h_m), balance height (h_0), nonlinear and linear neutral winds (U, U_l), the loss scale height factor (k), the diurnal coefficient c, and the diurnal period (M,D,E,N).

Changes Made from a Prior USU Servo Model

A previous USU Servo model was developed by Ballard

[1991]. Several changes have been made to this servo model.

The prior servo model was written in BASIC programming language. It required input files to be created for the ion number densities and the height of the F2 peak. The current servo model has been rewritten in FORTRAN programming. It incorporates the MSIS and IRI models as subprograms to obtain the ion composition and F2 peak heights. It has the added capability of reading files of F2 peak heights. These changes make this model easier to run and more accessible to the general user. Incorporating the IRI gives it a predictive capability for average trends.

The continuity equation diurnal coefficients (c) used in the new USU Servo model are tuned to the FLIP model. Zero winds were input into the FLIP model to obtain balance heights. These heights were then used to compute c values at numerous mid-latitude locations for both high and low values of solar activity and flux. This was done for both the equinoxes and solstices. The current model interpolates the values in these files for specific locations and times. The values are also interpolated for input F10.7 solar radio flux and Ap values.

These changes replace the balance height adjustments made in the previous USU Servo model. Balance heights were adjusted based on the initially assigned boundary condition

(dip angle = 90) values for c for daytime and nighttime periods (daytime: c=1, nighttime: c=1.3). Balance heights were then computed using these values. These balance heights were then adjusted to compensate for the decreased efficiency of plasma diffusion at smaller dip angles. The resulting balance heights were then used to calculate new coefficients. These new c values were used to recalculate balance heights used in the determination of the neutral winds.

CHAPTER IV

RESULTS

The USU Servo model is compared with measured neutral wind data from incoherent scatter radars and Fabry-Perot Interferometers. The linear meridional neutral wind calculation of the USU Servo model is used in all comparisons. (Buonsanto et al., [1989] showed that neutral winds derived from a servo model developed by Miller et al., [1986] were not significantly affected by an assumption of linearity between wind speed and the distance between hmF2 and the balance height.)

The USU Servo model comparisons are limited to a few days and for equinox periods only. The servo model is also compared with other models using different calculation techniques. These models include a meridional neutral wind model based on the Field Line Interhemispheric Plasma (FLIP) model [Richards and Torr, 1988; Miller et al., 1986]. Comparisons to the National Center for Atmospheric Research Thermosphere/Ionosphere General Circulation Model (TIGCM) [Roble et al., 1988] are also made.

The USU Servo model was run for the same periods using both an International Reference Ionosphere (IRI) depiction of the height of the maximum electron density in the F layer (hmF2) and measured hmF2 values to derive the neutral winds. The IRI hmF2 values are also compared to the

measured heights.

When the USU Servo model results (obtained using the IRI hmF2 values) are compared to measured winds, the expected agreement is in a general sense. Exact agreement is not expected since the USU model represents average results, based on ionospheric models' average conditions, rather than a single day as depicted in the actual measurements.

Comparisons of the Model Results with Wind Measurements

This study made use of the CEDAR (Coupling, Energetics, and Dynamics of Atmospheric Regions) Data Base at the National Center for Atmospheric Research (NCAR), which, along with the Millstone Hill Fabry-Perot, is supported by the National Science Foundation.

Fabry-Perot Interferometer (FPI) poleward meridional neutral winds measured at Millstone Hill, Massachusetts (46.6N 288.6E) and Arecibo, Puerto Rico (18.3N 293.3E) are compared to the neutral winds computed by the USU Servo model. Comparisons to incoherent scatter radar (ISR) data from Arecibo are also made.

Comparisons with FPI Data

In Figure 2, Millstone Hill Fabry-Perot Interferometer (FPI) measurements are compared to the servo model derived

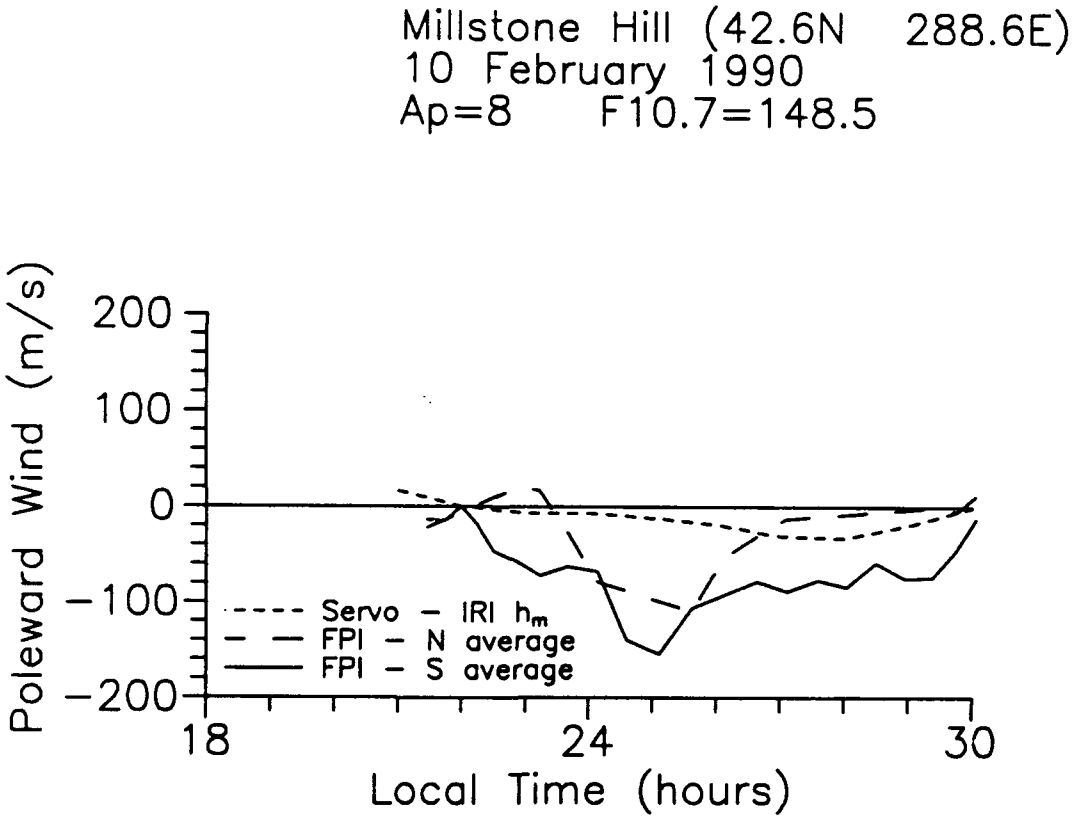

Fig. 2. Comparisons of the meridional neutral winds derived from the USU Servo model using IRI maximum heights of the F2 peak and Fabry-Perot Interferometer measurements. Data are from Millstone Hill for the night of 10 February 1990. The FPI data are averages of the northward and southward measurements.

neutral winds using layer heights from the IRI. The date of the measurement is 10 February 1990, a period of high solar activity.

The FPI equatorward winds approach 150 m/s. The servo-IRI winds portray a maximum of only 40 m/s. These servo model winds are 20-130 m/s weaker than the FPI winds. Agreement between these two winds is not expected since the servo model IRI-derived winds portray an average result, while the FPI winds represent a single day.

The average of the meridional neutral winds for 5, 6, 8, 9, and 10 October 1983 was obtained for Arecibo. This average represents a period of quiet geomagnetic activity and moderate solar activity. The Arecibo Fabry-Perot data were obtained from Dr. C. Tepley and Dr. R. Burnside [personal communication]. This average wind is compared to the servo-IRI model in Figure 3. The servo-IRI model follows the general trend of the FPI measured winds, except for the period around midnight. At this time the FPI winds increase equatorward while the servo-IRI winds increase poleward. The maximum difference between the two winds at this point is between 50-60 m/s. Figures 4 and 5 show a comparison of the servo-IRI winds with the FPI data at Arecibo, for a 15-16 March 1983 average and a 23, 26 December 1981 average. Again, the servo equatorward winds during the nighttime period show a maximum value of 40-60 m/s weaker than the FPI measured winds.

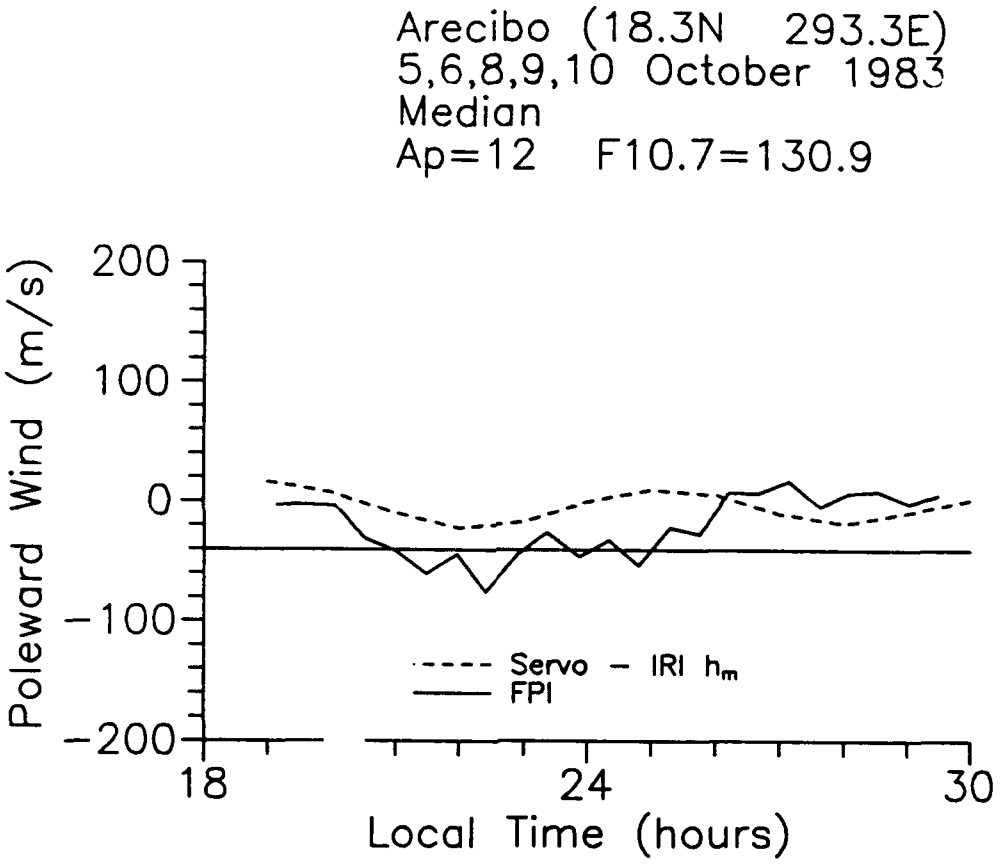

Fig. 3. Same as Figure 2 for Arecibo. Meridional neutral winds were averaged for 5, 6, 8, 9, and 10 October 1983.

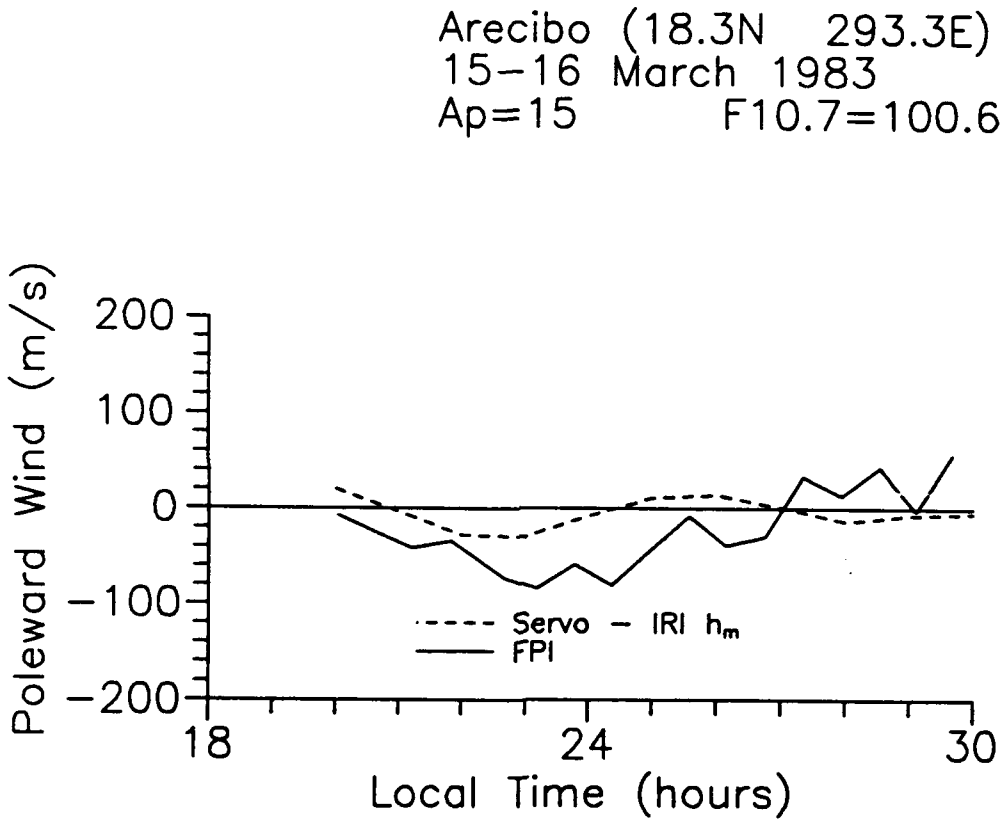

Fig. 4. Same as Figure 3 for Arecibo on 15-16 March 1983.

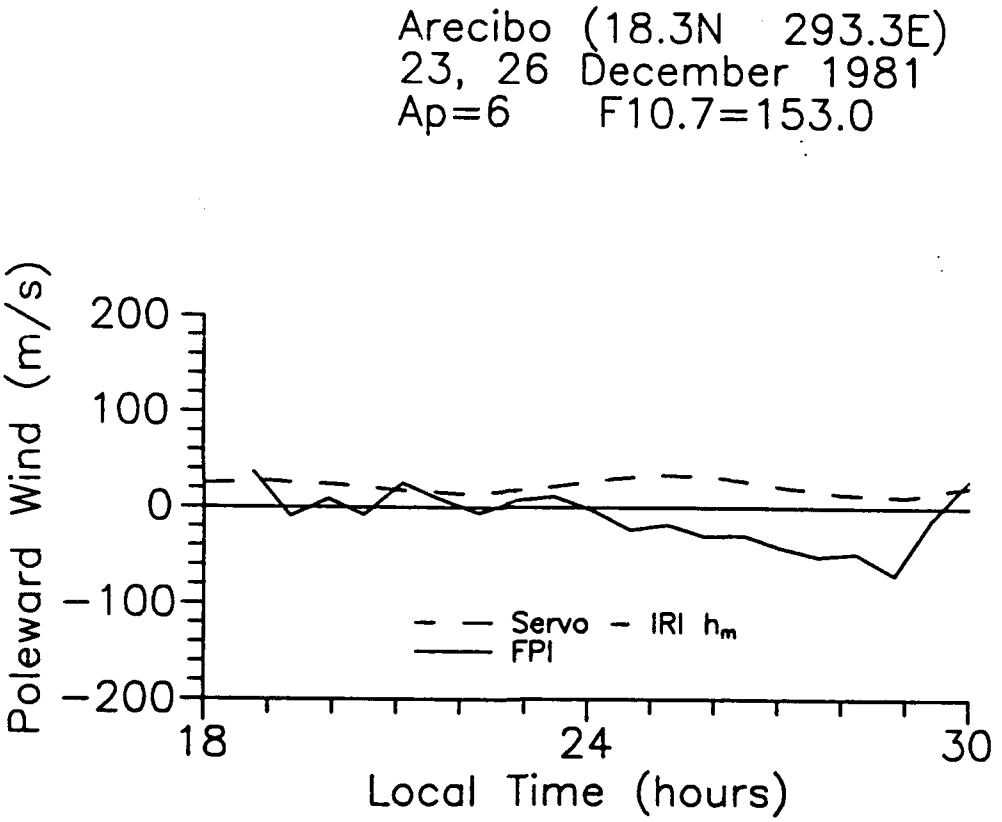

Fig. 5. Same as Figure 3 for Arecibo on 23 and 26 December 1981.

One must take into account that model average results, lacking day-to-day variability, are compared to single days of data. Another discrepancy between the two data sets arises from the different heights involved. Data obtained from Fabry-Perot Interferometer Doppler-shift measurements of airglow typically originate from about 50-70 km below the F2 peak. Also, electric fields affect lower-latitude locations such as Arecibo. These effects are not included in the USU Servo model development.

Comparisons with ISR Data

Data derived from incoherent scatter radar ion drifts from Arecibo for 19-20 September 1984 were obtained from Dr. R. Burnside [personal communication]. The data are compared to the servo IRI-derived winds and the servo hmF2-derived winds. These are shown in Figures 6 and 7. This represents a period of low solar activity.

High geomagnetic activity dominates this period, with a storm occurring on the 19th of September. This can be seen in the strong equatorward winds during the daytime of the 19th, approaching 200 m/s. Equatorward winds on the night of the 20th increase almost to 350 m/s.

The servo-IRI model does not account for these strong storm-induced equatorward winds. The wind differences can be seen in the divergences of the hmF2 values. However,

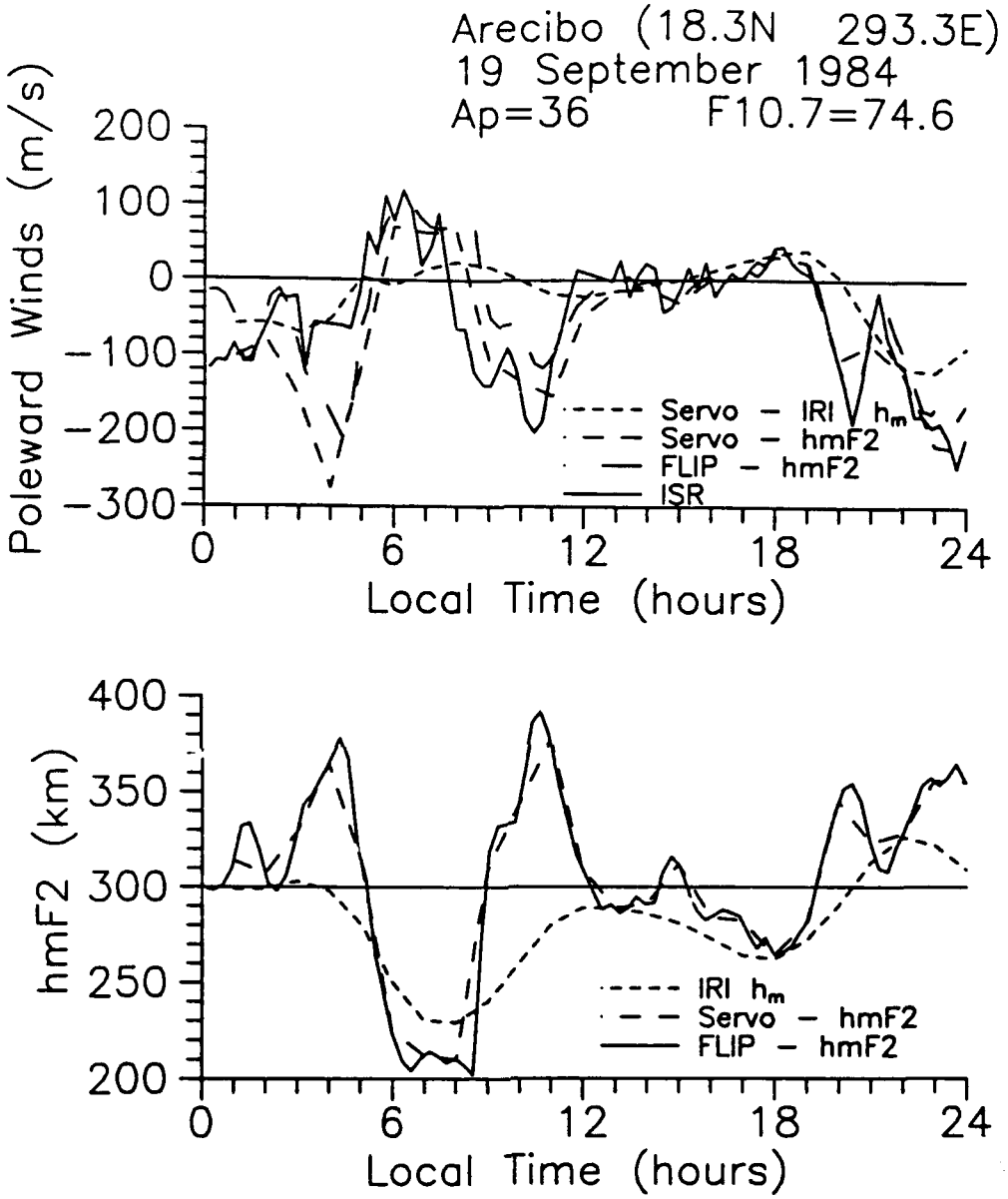

Fig. 6. Comparison of meridional neutral winds derived from the USU Servo model using IRI F2 peak heights, the USU Servo model using FLIP-derived winds, and incoherent scatter radar measurements. Data are for 19 September 1984.

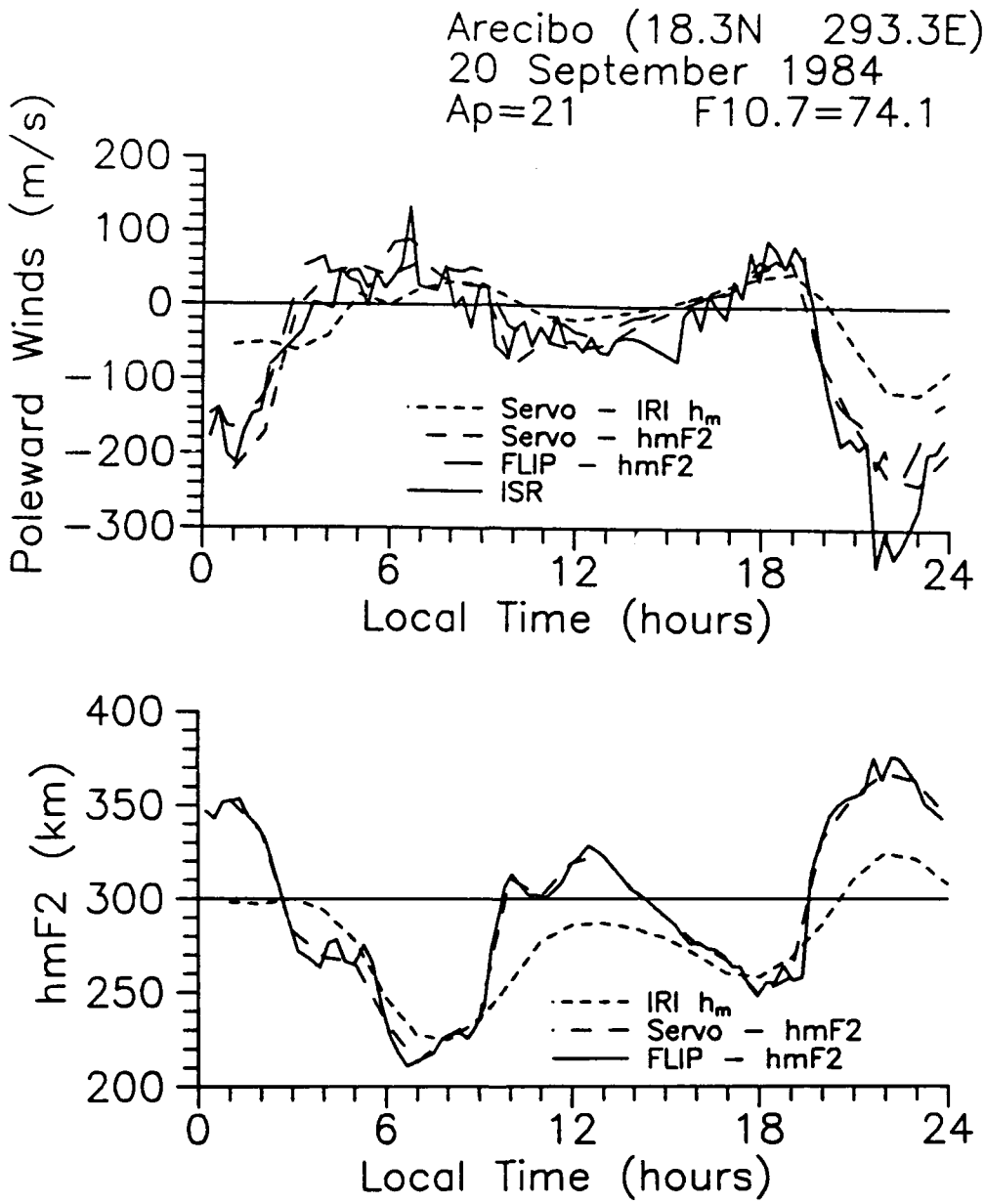

Fig. 7. Same as Figure 6 for 20 September 1984.

the general wind pattern is well represented by the servo model.

The servo hmF2-derived model closely follows the ISR derived wind data. It overestimates the strong equatorward winds on the morning and noontime of the 19th by 30-60 m/s.

In comparing the servo-IRI and the servo-hmF2 winds with the FLIP and ISR winds, it appears that if accurate heights are input into the USU Servo model, the resulting model runs also produce accurate neutral winds. The IRI averaged wind input into the USU Servo model naturally affects the smoothed neutral wind model output. The purpose of using the IRI model is the unavailability of widespread neutral wind measurements, along with the desire to obtain a general pattern for predicted winds. The IRI averaged heights also follow the actual wind patterns reasonably well.

Miller et al. [1987] compared neutral winds derived from incoherent scatter radar ion drift measurements with winds derived from the height of the F2 layer peak. They reasoned that since these wind derivations rely on average conditions from model calculations, there are natural errors involved. These inherent errors, along with uncertainties in the parameters used in the model calculations, might justify a realistic error bar as large as 50 to 75 m/s for neutral winds computed from the height of the F2 peak.

Comparisons of the Model Results with Other Models

In this section, poleward meridional neutral winds computed by the USU Servo model are compared to a FLIP-derived wind model [Miller et al., 1986] and the Thermosphere/Ionosphere General Circulation Model (TIGCM) [Roble et al., 1988].

Comparison to a FLIP-Derived Neutral Wind Model

The poleward meridional neutral winds derived from the USU Servo model are compared with a meridional neutral wind model based on the servo model of Rishbeth [1967] and Miller et al. [1986]. It uses the FLIP model to compute the parameters used. The winds are then derived from a measurement of the height of the F2 layer maximum electron density. The closely linear relationship between the F2 peak and the speed of the neutral winds is the basis of this method of obtaining the neutral winds. The FLIP-derived winds use hmF2 measurements from incoherent scatter radar and ionogram inversion techniques [Miller et al., 1986; 1989]. These winds are annotated as FLIP-derived winds on the graphs that follow. Comparisons of this method of obtaining the neutral winds were made by Miller et al. [1986; 1989] to Fabry-Perot interferometer and incoherent scatter radar data and were found to produce

favorable results.

Figures 8, 9, 10, and 11 depict winds and F layer peak electron density heights at four locations during periods of low solar activity and active geomagnetic conditions. These stations are Akita, Japan (39.7N 140.1E); Canberra, Australia (35.3S 149.0E); Khabarovsk, Russia (48.5N 135.2E); and Kiev, Ukraine (50.7N 30.3E). The winds are moderately strong and exhibit the general diurnal patterns of daytime winds and the FLIP-derived winds becomes larger.

During the day, the USU Servo model winds follow the FLIP-derived winds relatively well. The measured hmF2-derived servo winds are closer to the FLIP-derived winds. The maximum FLIP-derived winds are around 60-100 m/s. The daytime servo model IRI-derived winds differ from the FLIP-derived winds by a range from 0-50 m/s. This deviation is explained by the difference between the climatological IRI hmF2 values and the measured heights.

Figure 12 depicts a scatter plot of hmF2 values for the month of September 1986 for Canberra. This plot illustrates the variability of hmF2 values over a month. The heights at each hour varied from 20-70 km from the mean value over the course of the month. As noted earlier, if accurate heights are input into the USU Servo model, the resulting neutral wind calculations are also reliable.

At night, the disagreement between the servo model greatly exaggerates the equatorward winds. The servo-IRI

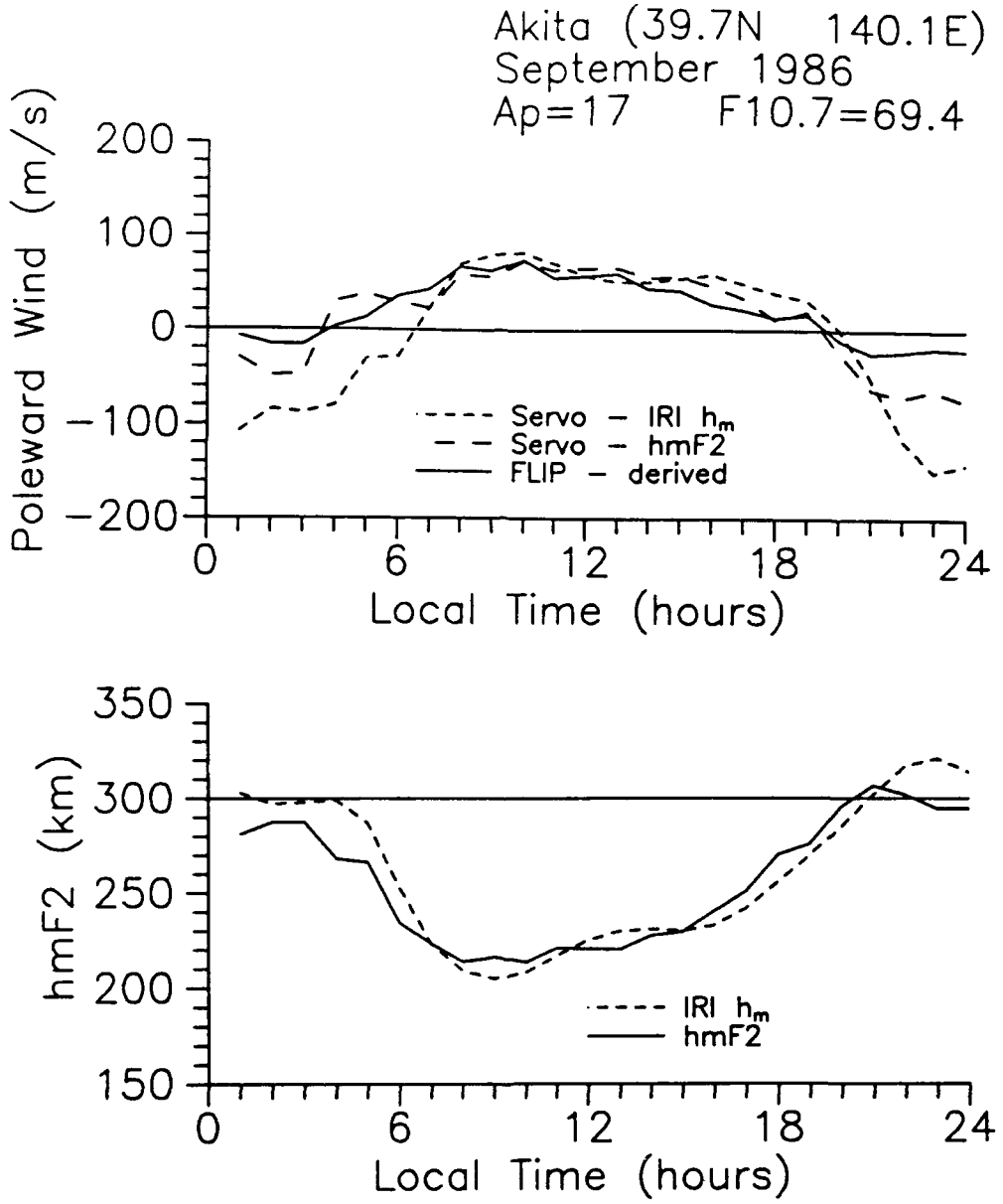

Fig. 8. Comparisons between the USU Servo model meridional neutral winds using IRI F2 peak heights, the USU Servo model neutral winds using ionosonde measured heights, and the neutral winds derived from the FLIP-derived model. The IRI heights are also compared to the measured heights. The data are a median for September 1986 for Akita.

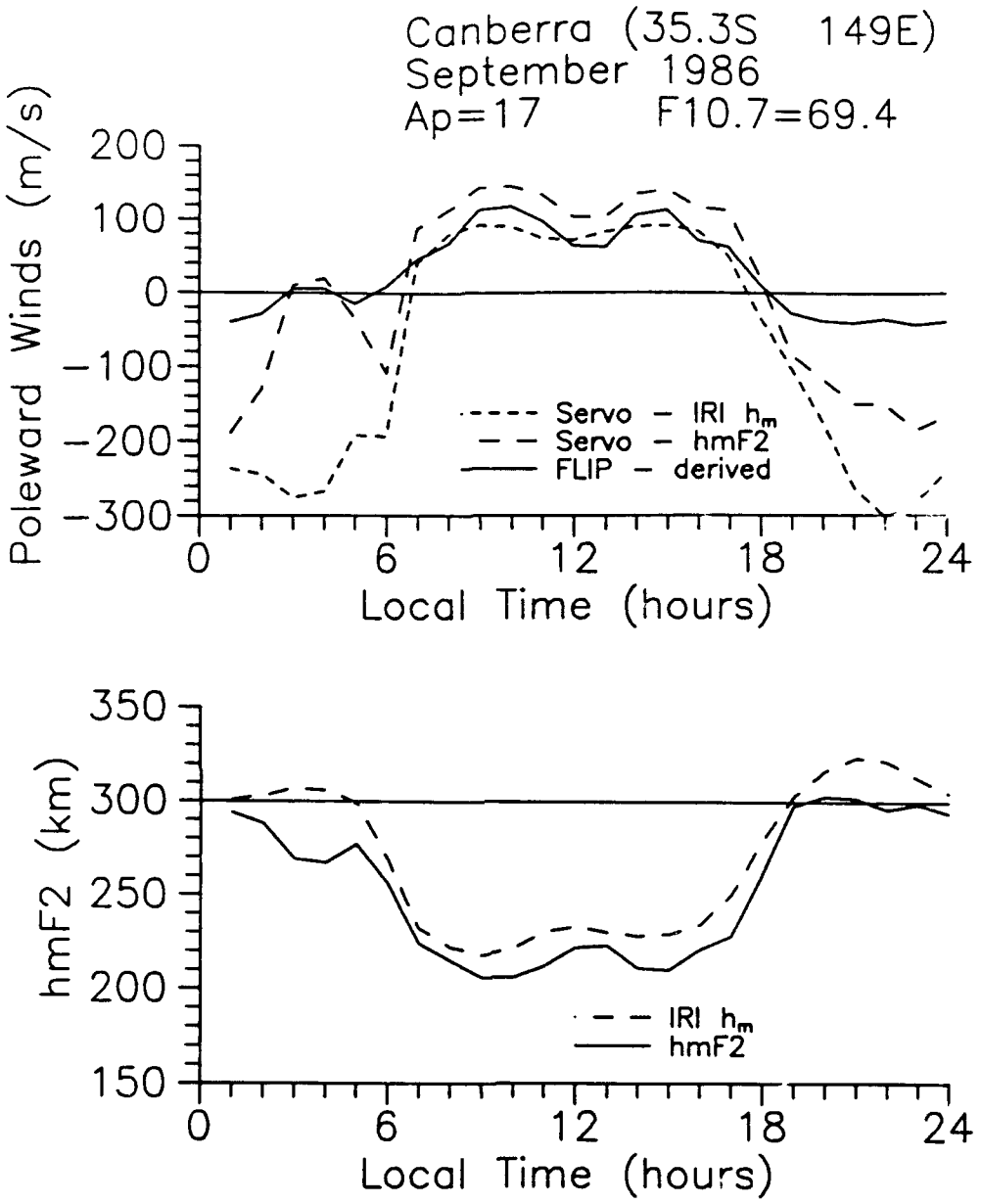

Fig. 9. Same as Figure 8 for Canberra.

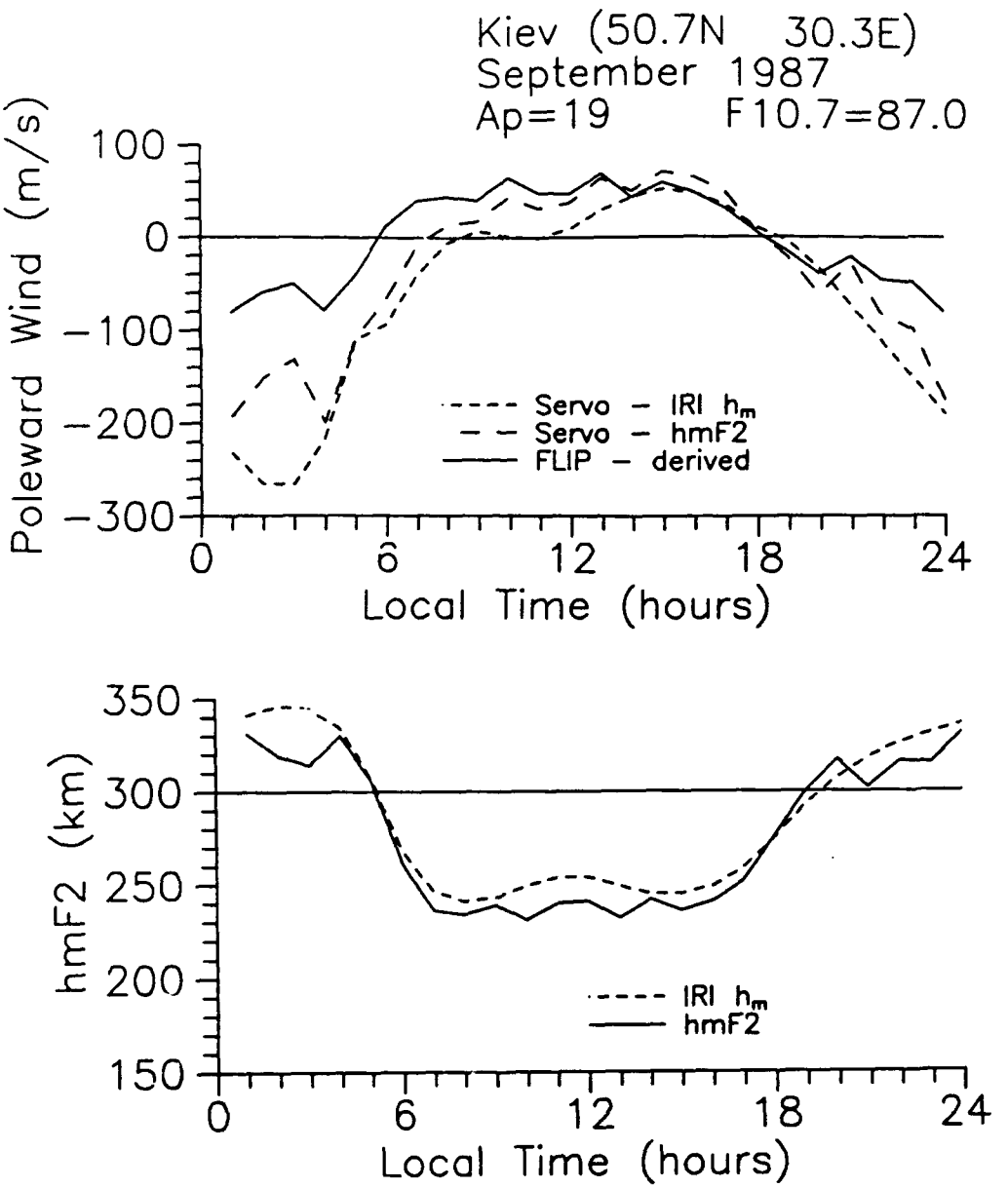

Fig. 10. Same as Figure 8 for Kiev. A median for September 1987 is shown.

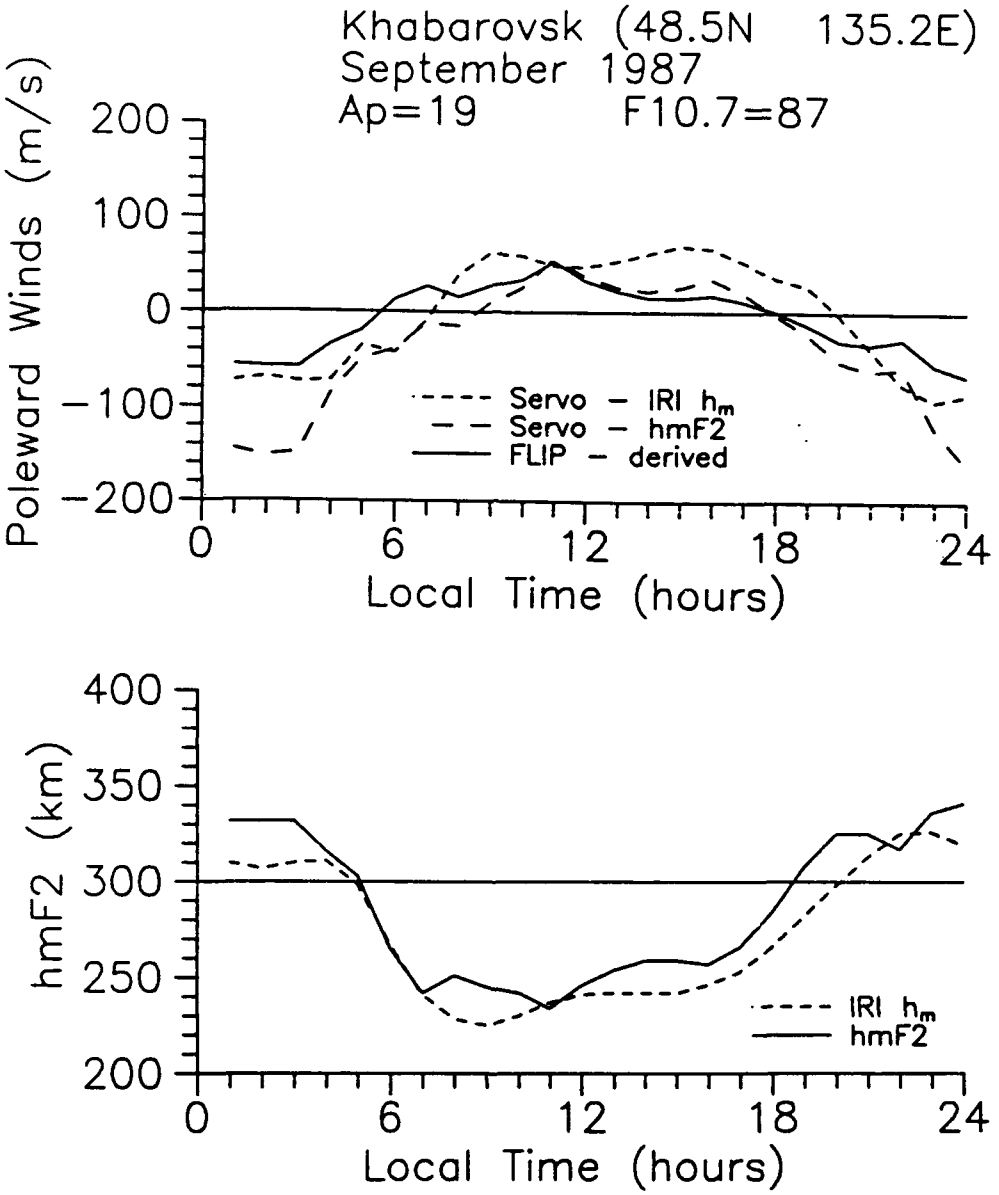

Fig. 11. Same as Figure 8 for Khabarovsk. A median for September 1987 is shown.

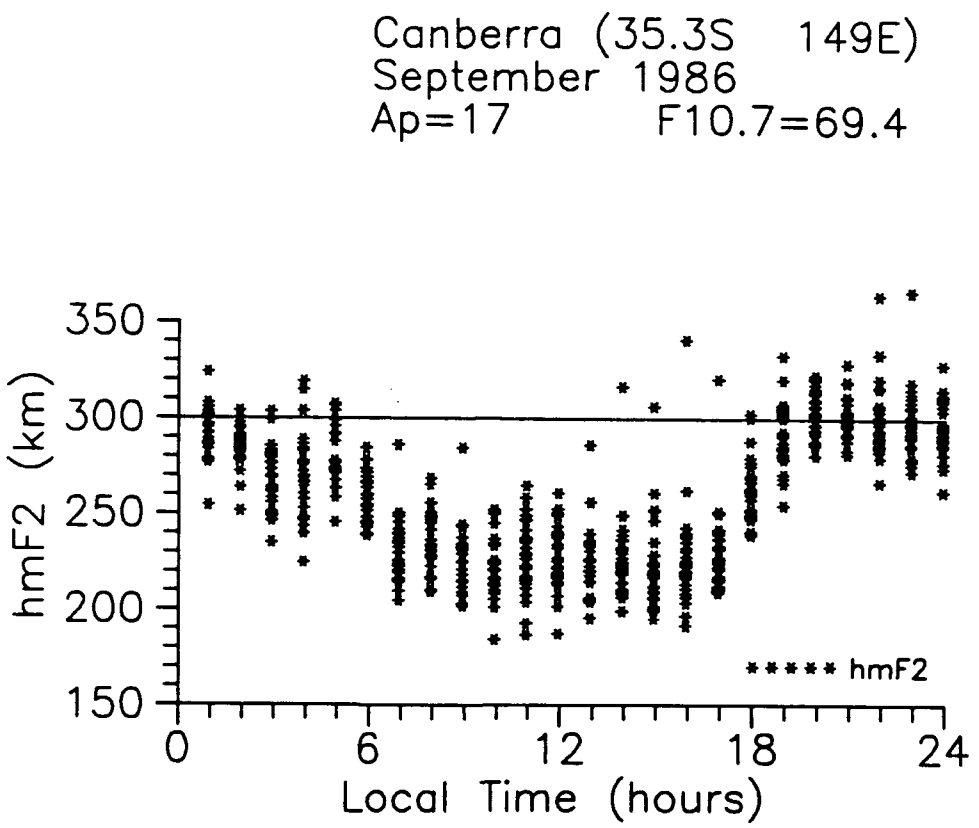

Fig. 12. Scatter plot of hmF2 values from Canberra for September 1986.

equatorward winds greatly exceed the winds produced by the FLIP derivation wind model, with maximum differences of 60-130 m/s and a maximum of over 300 m/s at Canberra. At the same time, the servo-IRI winds exceed the servo-measured hmF2 equatorward winds by 40-130 m/s, with a maximum of 300 m/s at Canberra. During this time, the difference between the IRI hmF2-derived servo winds and the measured hmF2-derived servo winds is explained by the differences in the respective heights.

One reason for the disagreement in the nighttime winds may be the increase in magnetic activity at these locations. During periods of increased magnetic activity, electric fields have a heightened effect on the vertical plasma drift [Rishbeth, 1971]. During these periods, the poleward perpendicular component of the ion drift velocity, $V_{\perp p}$, becomes more influential in determining the plasma drift, W. The equation for the plasma drift, which includes $V_{\perp p}$ is
equation (20):

$$W = V_{\perp p} \cos I - U_p \cos I \sin I \tag{44}$$

$$U_p = \frac{- V_{\perp p}}{W \sin I} \tag{45}$$

A westward perpendicular component of the ion drift, induced by electric fields, would then increase the poleward meridional neutral winds, thereby decreasing the

equatorward winds.

Another factor in the huge nighttime differences is the increased solar activity. This intensifies ion drag and therefore decreases the nighttime equatorward winds. Smaller differences in the daytime winds are due to the added increase in pressure gradients during high solar activity, balancing the ion drag force.

Figures 13 and 14 show comparisons during a period of high solar activity and a geomagnetically quiet time. These comparisons are at mid-latitude stations in both the northern and southern hemispheres: Akita and Canberra. The winds are relatively weak, with maximum winds at Akita of 40 m/s and 30 m/s at Canberra.

Winds tend to decrease during periods of increased solar activity. Although higher solar activity results in enhanced solar radiation, causing increased differential heating and therefore higher pressure gradients and stronger winds, high solar activity also results in an increased photoionization rate. The resultant higher concentration of ions produces greater numbers of ion-neutral collisions and therefore increased ion drag. This occurs since ion drag increases more rapidly than the pressure gradient during periods of higher solar activity [Rishbeth, 1972].

The climatological IRI hmF2 values follow the measured heights well, with a maximum difference of 25 m/s at noon.

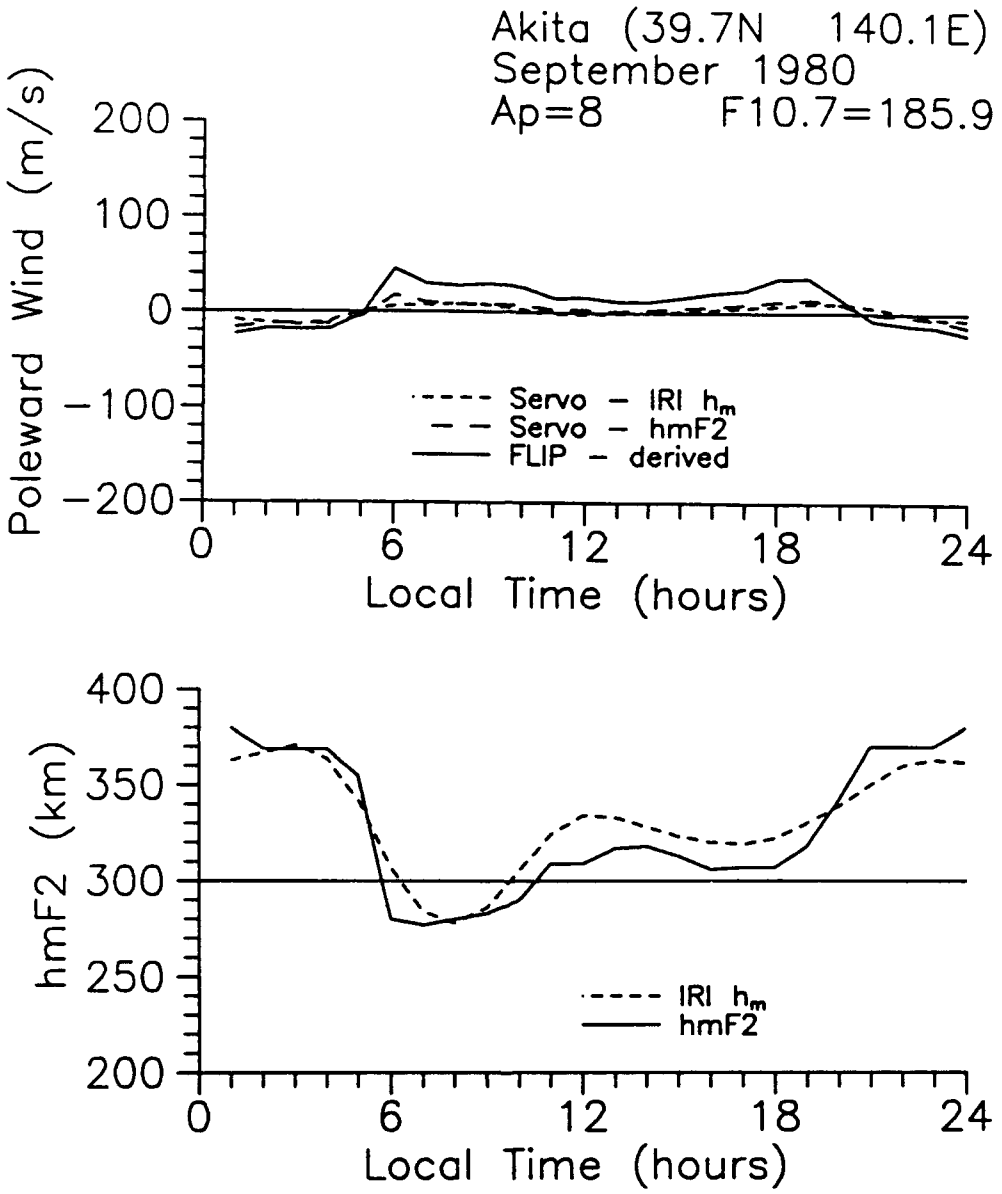

Fig. 13. Same as Figure 8 for Akita. A median for September 1980 is shown.

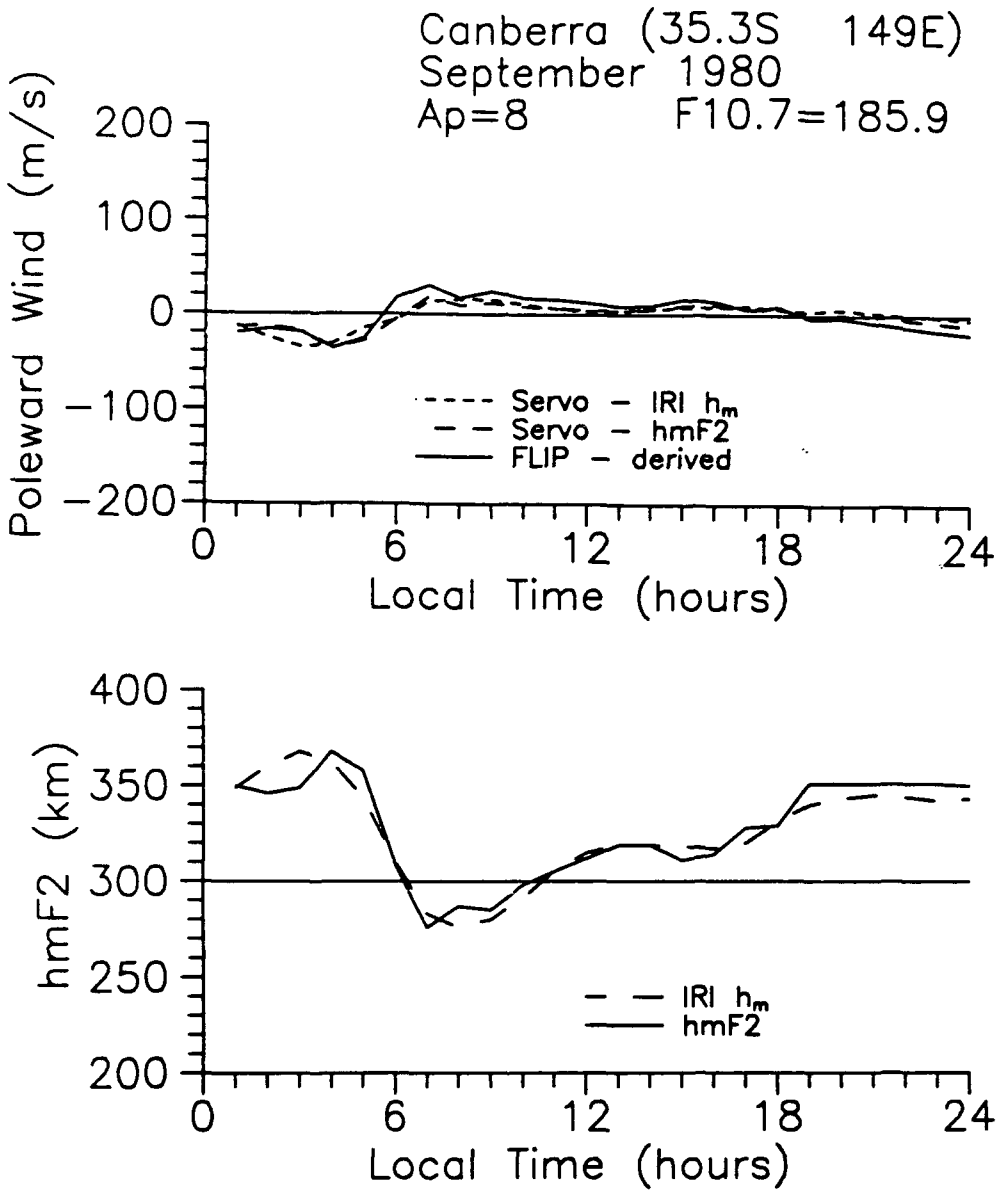

Fig. 14. Same as Figure 13 for Canberra.

The winds from the servo model using the measured hmF2 values are almost identical to the FLIP-derived winds. The servo model winds using IRI hmF2 values closely follow the FLIP-derived and the measured hmF2 servo winds. At Akita, the winds are 20-40 m/s stronger in the daytime, with the greatest difference occurring at sunrise and sunset.

Comparisons with the TIGCM
Meridional Neutral Winds

The National Center for Atmospheric Research Thermosphere/Ionosphere General Circulation Model (TIGCM) [Roble et al., 1988] is a Eulerian model of the global structure of the ionosphere and the thermosphere. It is self-consistent and agrees reasonably well with empirical models (MSIS-86) [Roble et al., 1988]. The TIGCM data were obtained from Dr. Cassandra Fesen [personal communication]. Four locations were compared to the TIGCM for March 1990. The results are shown in Figures 15 and 16. This was again a period of high solar activity.

The servo-IRI winds compare favorably with the TIGCM at Canberra. Differences in wind speeds range from 10 to 20 m/s. The servo nighttime equatorward winds approach a difference of 40 m/s.

At Akita, the TIGCM daytime poleward winds exceed the servo winds by a maximum of 40 m/s. The TIGCM nighttime equatorward winds are 50-80 m/s stronger than the servo winds at this time.

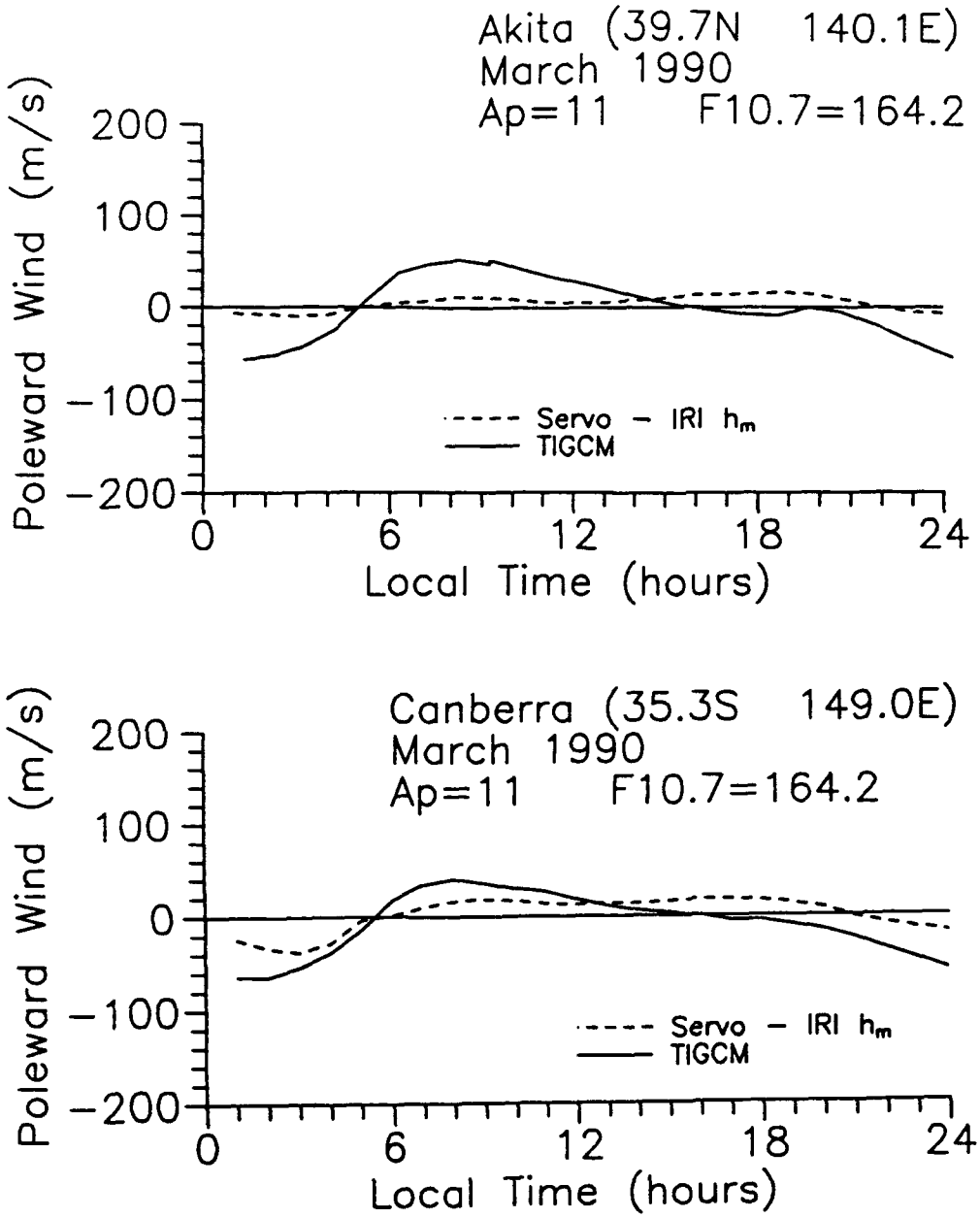

Fig. 15. Comparisons between the USU Servo model meridional neutral winds using the IRI F2 peak heights and the TIGCM model neutral winds. The data are for Akita and Canberra for March 1990.

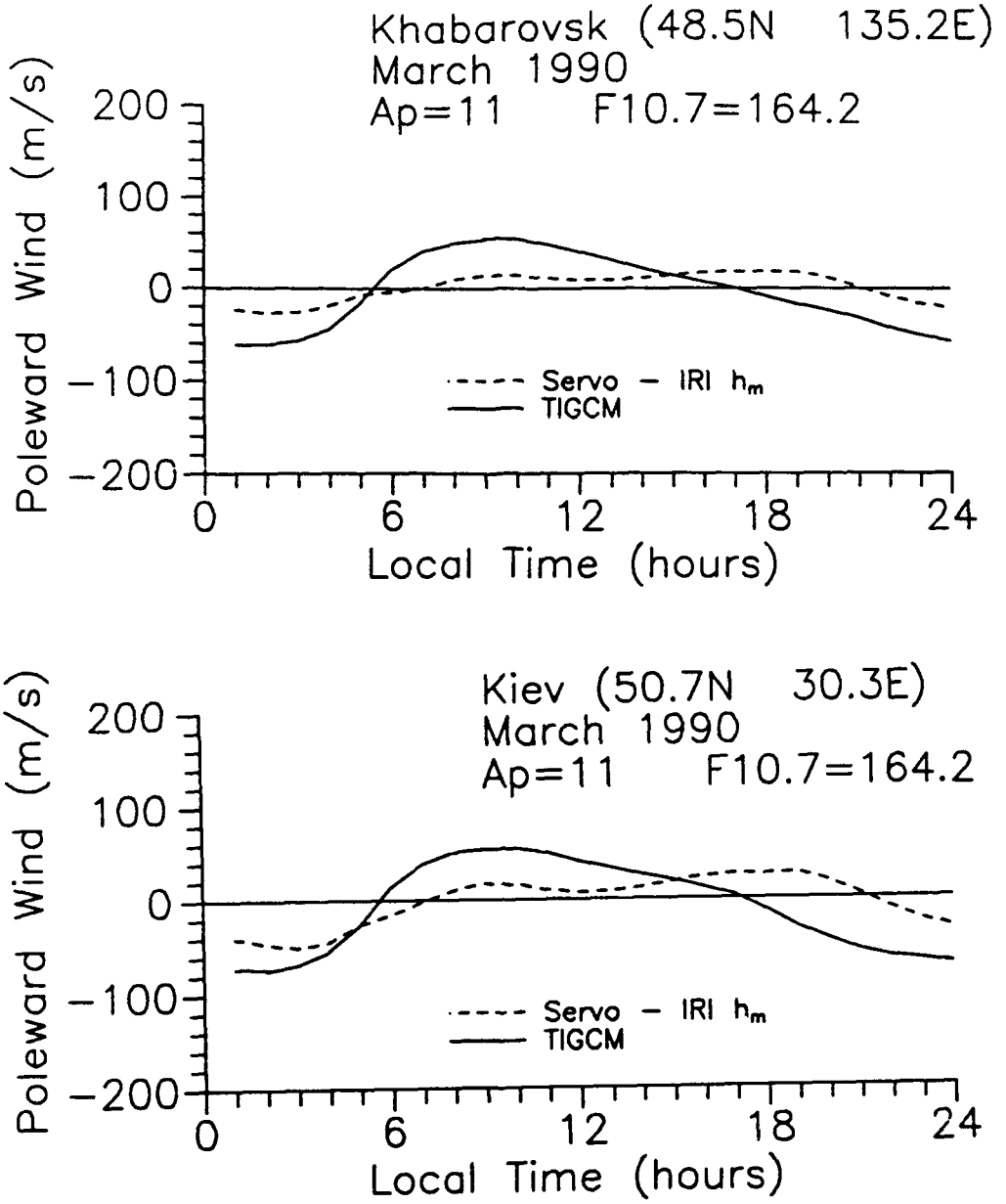

Fig. 16. Same as Figure 15 for Khabarovsk and Kiev.

In Figure 15, these differences are again reproduced at Khabarovsk and Kiev.

The comparisons between the USU Servo model and ISR and FPI neutral wind data were performed to highlight any significant programming errors made in the development of the USU model. By acknowledging the smoothing properties and the noninclusion of electric field effects in the USU model, general wind patterns were reproduced. Comparisons with other ionospheric models were also useful indetermining the on-track perspective of the continuing development of the USU model. Also, the relative accuracy of the IRI averaged heights validates the use of the USU Servo model as a predictive tool for average winds.

CHAPTER V

CONCLUSIONS

The USU Servo model provides a quick, valuable tool to calculate mid-latitude meridional neutral winds from the height of the F2 peak. The principal equations are based on a servo model developed by Rishbeth et al. [1978] to study the effect of plasma drift velocity on the F2 peak.

The fundamental concept behind the servo model is that the change in the F2 peak, which is at a balance height between chemical processes and diffusion, is a result of a wind-induced change in that equilibrium. Heating from solar EUV and UV absorption primarily determines the circulation in the F region during quiet geomagnetic conditions. Horizontal temperature differences induce horizontal pressure gradients, generating winds. Poleward winds, occurring primarily in the daytime, induce a downward ionization drift, in effect lowering the F2 layer. Conversely, equatorward winds, usually occurring at night, drive the ionization up the field lines, pushing the F2 layer upward and raising the F2 peak.

The USU Servo model can be run in either an interactive mode, with program-directed data inputs, or by a file containing the desired parameters. The model incorporates the Mass Spectrometer Incoherent Scatter (MSIS) model [Hedin, 1987] to depict the neutral

atmosphere. The USU Servo model uses molecular and atomic number densities and neutral temperature values from the MSIS model. The height of the maximum electron density in the F2 layer (hmF2) is obtained from the International Reference Ionosphere (IRI) [Bilitza et al., 1987] and is also included in the USU Servo model. The IRI gives empirical monthly averages of hmF2 for magnetically quiet conditions.

The USU Servo model contains a data base of diurnal coefficients for numerous locations and various atmospheric conditions. This data base was calculated from balance heights obtained from a zero wind input into the Field Line Interhemispheric Plasma (FLIP) model [Richards and Torr, 1985]. The input parameters are used to interpolate between these diurnal coefficient data files, to obtain the best approximation. The most significant reason for choosing the USU Servo model over the FLIP model to obtain the neutral winds is the computational speed of the servo model. The FLIP model takes considerably longer to obtain results, whereas the USU Servo model can be run in a matter of minutes.

The USU Servo model is a convenient, moderately accurate means of obtaining mid-latitude meridional neutral winds. For geomagnetically active periods and for lower latitudes, the biggest uncertainty of the USU Servo model arises from induced plasma motions from electric fields.

Inclusion of the IRI gives the USU Servo model a predictive capability for general trends expected under various conditions. Although the IRI portrays only climatological heights of the maximum electron density, it has, when combined with the USU Servo model, shown itself to be a good predictor of general meridional neutral wind patterns. For areas and times when measured hmF2 data are not available, the inclusion of the IRI into the USU Servo model is proven to be useful.

The most significant limitation of the USU Servo model is the averaging effects of its neutral wind output. Another factor is its treatment of the F2 layer as a single entity. Other limitations include its nonapplicability to the low and high latitudes and its noninclusion of electric field-induced plasma motions during high geomagnetic activity and at low and high latitudes.

I suggest that additional comparisons be made between the USU Servo model and the Fabry-Perot Interferometer and incoherent scatter radar data at night. This would determine the reasons for the nighttime discrepancies and develop corrections that can be made to the nighttime diurnal coefficients. Also comparisons should be made during solstice periods. I recommend that additional diurnal coefficient data files for more locations and additional atmospheric corrections be derived from the FLIP

model. This would increase the accuracy of these diurnal coefficients.

REFERENCES

Ballard, T., The Calculation of Mid-Latitude Meridional Neutral Winds From an Improved Servo Model Approximation Method, M.S. Thesis, CASS Report #91-03-01, Utah State University, Logan, UT, 1991.

Bilitza, D., International Reference Ionosphere 1990, National Space Science Data Center, Lanharm, MD, 1990.

Bilitza, D., K. Rawer, S. Pallaschke, C. M. Rush, N. Matuura, and W. R. Hoegy, Progress in modeling the ionospheric peak and topside electron density, Adv. Space Res., 7, 5, 1987.

Buonsanto, M. J., J. E. Salah, K. L. Miller, W. L. Oliver, R. G. Burnside and P. G. Richards, Observations of neutral circulation at mid-latitudes during the equinox transition study, J. Geophys. Res., 94, 16,987, 1989.

Hedin, A. E., MSIS-86 Thermospheric model, J. Geophys. Res., 92, 4649, 1987.

Kelley, M. C., The Earth's Ionosphere, Plasma Physics and Electrodynamics, Academic Press, Inc., San Diego, CA, 1989.

Lutgens and Tarbuck, The Atmosphere, Prentice-Hall Inc., Englewood Cliffs, NJ, 1986.

Miller, K. L., D. G. Torr, and P. G. Richards, Meridional winds in the thermosphere derived from measurement of the F2 layer height, J. Geophys. Res., 91, 4531, 1986.

Miller, K. L., J. E. Salah, and D. G. Torr, The effect of electric fields on measurements of meridional neutral winds in the thermosphere, Annales Geophysicae, 5, 337, 1987.

Miller, K. L., P. G. Richards, and D. G. Torr, The derivation of meridional neutral winds in the thermosphere from F2-layer height, in World Ionosphere/Thermosphere Study Wits Handbook, vol. 2, edited by C. H. Liu, pp. 439-471, SCOSTEP, University of Illinois, Urbana, IL, 1989.

Prlöss, G.W., L. H. Brace, H. G. Mayr, G. R. Carignan, T. L. Killeen, and J. A. Klobuchar, Ionospheric storm effects at subauroral latitudes: A case study, J. Geophys. Res., 96, 1275, 1991.

Richards, P. G., An improved algorithm for determining neutral winds from the height of the F2 peak electron density, J. Geophys. Res., 96, 17,839, 1991.

Richards, P. G., and D. G. Torr, Seasonal, diurnal and solar cycle variations of the limiting H^+ flux in the Earth's topside ionosphere, J. Geophys. Res., 90, 5261, 1985.

Richards, P. G., and D. G. Torr, Ratio of photoelectron to EUV ionization rates for aeronomic studies, J. Geophys. Res., 93, 4060, 1988.

Richmond, A. D., Thermospheric dynamics and electrodynamics, in Solar-Terrestrial Physics, edited by R. L. Carovillano and J. M. Forbes, pp. 523-607, D. Reidel Publishing Company, Dordrecht, Holland, 1983.

Rishbeth, H., The effect of winds on the ionospheric F2-peak, J. Atmos. Terr. Phys., 29, 225, 1967.

Rishbeth, H., Polarization fields produced by winds in the equatorial F region, Planet. space Sci., 19, 357, 1971.

Rishbeth, H., Thermospheric winds and the F-region: A review, J. Atmos. Terr. Phys., 34, 1, 1972.

Rishbeth, H., Basic physics of the ionosphere: A tutorial review, J. IERE, 58, S207, 1988.

Rishbeth, H. and O. K. Garriott, Introduction to Ionospheric Physics, Academic Press, Inc., New York, 1969.

Rishbeth, H., S. Ganguly, and J.C.G. Walker, Field-aligned and field-perpendicular velocities in the ionospheric F2-layer, J. Atmos. Terr. Phys., 40, 767, 1978.

Roble, R. G., Dynamics of the Earth's thermosphere, Rev. Geophys. Space Phys., 21, 217, 1983.

Roble, R. G., E. C. Ridley, A. D. Richmond, and R. E. Dickinson, A coupled thermosphere/ionosphere general circulation model, Geophys. Res. Lett., 15, 1325, 1988.

Schunk, R. W., The terrestrial ionosphere, in Solar-Terrestrial Physics, edited by R. L. Carovillano and J. M. Forbes, pp. 609-676, D. Reidel Publishing Company, Dordrecht, Holland, 1983.

Sojka, J. J., and R. W. Schunk, A theoretical study of the global F region for June solstice, solar maximum, and low magnetic activity, J. Geophys. Res., 90, 5285, 1985.